Compact & Lightweight Antenna Designs for Harmonic Radar Application

ZE FU
HAMZA BIN FAHEEM
MASTER´S THESIS
DEPARTMENT OF ELECTRICAL AND INFORMATION TECHNOLOGY
FACULTY OF ENGINEERING | LTH | LUND UNIVERSITY

Compact & Lightweight Antenna Designs for Harmonic Radar Application

Ze Fu & Hamza Bin Faheem

Department of Electrical and Information Technology
Lund University

Supervisor: Prof. Anders J Johansson

Examiner: Prof. Fredrik Rusek

September 30, 2018

Printed in Sweden
Tryckeriet i E-huset, Lund

Abstract

The purpose of this paper is to design a new lightweight and compact antenna system for harmonic radar applications to be used to trace the migration of the Bogong moths.

The main approach adopted in this paper to solve this problem is to build three antennas suitable for use in real environment, where the modeling and the simulations were done in CST Microwave Studio Suite 2018. The principle applied in the system to identify and track a target is to transmit a fundamental wave signal f_0 in X-band and receive its harmonic response signal at a frequency $2f_0$ with the help of a transponder that is fitted on the target and has non-linear characteristics. The overall link budget of the power consumption and conversion efficiency of the transponder are analyzed towards to the end.

The results obtained in this research include the design of an 8×8 microstrip patch antenna array for transmission at 9.41GHz having 21.1 dBi of gain and measures $143.5 \times 140.5\ mm^2$; an 8×16 microstrip patch antenna array for reception at 18.82 GHz having 24.5 dBi of gain and measures $143.5\times\ 76\ mm^2$; A dual-band folded dipole design was chosen for the transponder which was approximately 30 mm in length, had a thickness of 0.005 mm and an estimated -13.41 dBi(21.35%) conversion efficiency in the ideal case. The effects of choosing different substrates for such arrays are also discussed.

The impact of our obtained results provides a new solution for tracking insects which were previously deemed to be too weak due to their poor load carrying capabilities such as the Bogong moths. We have also presented a MATLAB model to estimate the conversion efficiencý of a transponder for the general case .

Popular Science Summary

Billions of Bogong moths migrate from the parched plains of Australia to the countries' south-eastern Alps in every spring in order to avoid the menacing heat by hiding in caves where they remain dormant over the summer. Come autumn, the journey back to the birthplace begins, where upon return, mating takes place, followed by the laying of eggs and finally death. The caterpillars that hatch out of the eggs develop underground through winter and carry the same routine all over again.

Exactly how an insect can make this months' long epic journey, hundreds of miles, back and forth, in the dark of the night with such regularity has been baffling for biologists, let alone the fact it is a journey they have never made before to a place they have never seen before. In a paper published recently in current biology [1], it has been tested and proved that moths use magnetic fields like a compass when they were exposed to visual cues and magnetic fields inside an outdoor flight simulator, although this experiment was not very successful as the moths got confused after a few minutes and so the mystery continued. The only other insect species to make such a long, directed and specific migration is the monarch butterfly but unlike them who navigate by using the reliably rising and setting sun, these moths fly at night beneath the wishy-washy constellations using their magnetic compass.

To solve this mystery a high tech radar scanning system was proposed which has been previously used to track birds and other large insects to some extent. Now one might wonder how such a system can be placed on a tiny and weak insect but that is where the latest antenna simulation technology comes into play. A harmonic radar was designed which consisted of a transmitting antenna and a receiving antenna, both of which were to be attached to a drone which could then track the insect. On the insect end, the task was very challenging because a high powered drone could carry a battery source to run the radar equipment, a Bogong moth cannot carry over 15 milligrams of weight. To solve this issue, an electronic component called a beam lead Schottky barrier diode is used on a miniature folded dipole antenna of roughly 15 millimeter length, which instead of using a power source, makes use of the non-linear nature of the diode i.e. when an interrogating signal from the transmitter on the drone hits this miniature antenna, the diode reflects back a signal at double the frequency which can then easily be

detected by the receiver on top of the drone. Preliminary tests were carried out in the communications research laboratory at LTH to verify the results that were simulated on an electromagnetic simulator software and now the project is moving towards the actual testing phase in the field.

Table of Contents

List of Figures

List of Tables

Chapter 1

Introduction

This project comprised of two major design tasks. The first one being the design and simulation of a multiple patch antenna system for the harmonic radar and the second one being the design and simulation of the transponder to be attached to the flying insect. The major design restriction was regarding the size in both cases which had to be under 210 x 210 mm in case of the multiple antenna system to be mounted on the drone tracking the flying insects whereas the transponder had to be small and light enough so that it does not impede the insects' flight performance and behavior when mounted on their back.

The simulations were done using CST Studio Suite 2018. The principles applied and the methodologies used will be explained in detail later on in this report but in a nutshell, a Harmonic radar is a radar system which can identify and track a target by transmitting the fundamental wave signal f_0 and receiving a harmonic response signal at frequency nf_0 with the help of a reflector. In these systems, the reflector (antenna on the target) is known as the harmonic transponder. The idea being that the transponder receives the interrogatory fundamental frequency signal from the radar and converts it to a harmonic signal through a nonlinear element embedded into it and sends it back. This makes the harmonic radar less susceptible to environmental clutter keeping it unobscured from reflections by its surroundings as most natural objects do not exhibit non-linearity and can only reflect back at the incident frequency. The nonlinearity aspect is introduced into the system with a diode which carries out the principle mentioned above producing harmonics of the RF energy incident on it. The center frequency was chosen to be 9.41 GHz which falls in the 9.225-9.500 GHz band which is reserved for Maritime Radar but has an exemption from the license requirement. The signal reflected back will be at 18.82 GHz i.e. the second harmonic. The transponder design is truly environmentally friendly and does not make use of a wire or dipole design and instead uses an organic substrate and a minimal foil antenna made of copper so that it does not hinder the insects' movement and is easily digested by any predator out in the wild.

Chapter 2

Background, Previous Work & Motivation

The principle of Harmonic Radar to track the movements of insects was first used in 1986 by Daniel Mascanzoni and Henrik Wallin at the Swedish University of Agricultural Sciences, Uppsala, Sweden [1]. Since then, tracking land dwelling as well as flying insects has been the topic of active research, mainly focused on pests harmful to agricultural industries around the world and extensive studies have been conducted to better control the population of such species.

Recent research in this area has been used for tracking insects such as Emerald Ash Borer, Honeybee, Colorado Potato Beetle, Black Vine Weevil, Asian Yellow-legged hornet etc. [1 2 3 4] but little attention has been given to make antenna designs environmentally friendly. The wire dipole (loop) design most commonly used in previous studies can be extremely harmful and in most cases kill the predator preying on the interrogated subject. The main motivation is to make advanced research and use suitable materials for the transponder design that will not do such harm to the ecosystem.

The famous work done by Colpitts and Boiteau made use of the wire loop dipole design shown in [3]. The concept used will be the same but due to the environmental restrictions mentioned earlier, we cannot use the same material and shape. The performance of the transponder can be improved though by using materials that yield a lighter structure while maintaining the same electrical output. Another study was made using the same dipole antenna design in [5] which involved a team from Lund University's department of ecology. The main antenna design was a 16 mm (6 mg) tag but the objective back then was just to demonstrate the potential of harmonic radar to investigate the flight of moths. The complexity of the implemented antennas varies a lot in terms of geometry in [6], [7] and [8] and the performance results from these studies will be vital to optimize/match the diode impedance directly to the load at the desired fundamental and harmonic frequencies and also to get an idea of how the simulation and actual physical test results compare with others around the world.

Chapter 3

Basic Definitions & Parameters

The IEEE defines an antenna as "that part of a transmitting or receiving system that's is designed to radiate or to receive electromagnetic waves." [Sec. H.2:"IEEE Standard Definitions of Terms for Antenna"]
In this chapter, some basic parameters are introduced which are almost always used in antenna theory with the reference from [11].

3.1 Radiation Pattern, $F(\theta, \Phi)$

It is defined as the graphical representation of an antenna's radiation properties as a function of space. It shows how an antenna is radiating energy out into space or how it is receiving energy from space. The gain of an antenna is mostly determined in the far field region (distances large compared to the size and wavelength of the antenna). The radiation pattern can be described with the help of azimuth and elevation plane patterns where the former term refers to "the horizontal" and the latter term refers to "the vertical".

3.2 Antenna Efficiency, e_0

Antenna efficiency refers to the ratio of the power radiated by the antenna to the active power input to the antenna. The value of total efficiency e_0 takes into account the losses at the input terminals and within the structure of the antenna. The losses may be due to:

- Reflections because of the mismatch between the transmission line and the antenna.
- I^2R losses (conduction and dielectric)

The overall efficiency is given by:

$$e_0 = e_r e_c e_d \tag{3.1}$$

Where:
e_0 = total efficiency
e_r = reflection efficiency = (1-$|\Gamma|^2$), where Γ is the voltage reflection coefficient at the input terminals of the antenna. $\Gamma = (Z_{in} - Z_0)/(Z_{in} + Z_0)$

Z_0 = the characteristic impedance of the transmission line. e_c = conduction efficiency
e_d = dielectric efficiency
Antenna efficiency is a measure of how well the feed network and the antenna are matched.

3.3 Gain, $G(\theta, \phi)$

The ratio of the power gain of an antenna in any given direction to the power gain of a reference antenna in the very same direction is known as the gain of that antenna. The gain usually considered is in the direction of maximum radiation (maximum gain). It takes into account the efficiency of an antennas as well as the directional capabilities. Gain of antenna is given by:

$$G(\theta, \phi) = e_r(\theta, \phi) \tag{3.2}$$

The gain of an antenna can also be defined as 4π times the ratio of the maximum radiation intensity in a given direction to the net power accepted by the antenna from the transmitter:

$$Gain = 4\pi \frac{\text{radiation intensity}}{\text{total input (accepted) power}} = 4\pi \frac{U(\theta, \phi)}{P_{in}} \tag{3.3}$$

And the relative gain is given by:

$$Gain = \frac{4\pi U(\theta, \phi)}{P_{in}(\text{lossless isotropic source})} \tag{3.4}$$

Which is the ratio between the power gain in a given direction to the power gain of a referenced antenna in a referenced direction.

3.4 Directivity, $D(\theta, \phi)$

An antenna has different radiation or reception capabilities in different directions of the space, this is called the antenna directivity. It is a parameter describing how much the radiation pattern of an antenna is directional. It is a characteristic of the radiated field of the antenna in the far field, and defined as the ratio of the radiation intensity in a given direction to the averaged isotropic radiation intensity, written as:

$$G(\theta, \phi) = e_r D(\theta, \phi) \tag{3.5}$$

3.5 Voltage Standing Wave Ratio

The measure of how much power is being delivered to a device against how much power is being reflected back by that device is called the voltage standing wave ratio. In other words, in a standing wave pattern, it is the ratio of the maximum voltage to the minimum voltage, so it tells us how perfectly the antenna is matched

to 50 Ω (matching of source and load impedance). The voltage standing wave ratio is given by:

$$VSWR = \frac{1 + |\Gamma|^2}{1 - |\Gamma|^2} \tag{3.6}$$

3.6 Beamwidth

The beam size between the angles at which the radiation pattern $F(\theta, \phi)$ is 10-dB below its peak value. The most widely used beam widths is the 3-dB beam width (half power beam width) which IEEE defines as " In a plane containing the direction of the maximum of a beam, the angle between the two directions in which the radiation intensity is one-half value of the beam." Hence, in other word it is basically the angular separation between two identical points on either side of $F(\theta, \phi)$ max.

Chapter 4

Designing the Microstrip Patch

Patch antennas are extremely popular for applications where size, weight and cost are the major constraints. Usually, it is a very thin $h_t \ll \lambda_0$, where 0 is the free space wavelength) rectangular patch (radiating element) of metal photo-etched on a thin ($h_s \ll 0$, usually $0.0030\lambda_0 \leq h \leq 0.050\lambda_0$) layer of the dielectric substrate which is sandwiched in between the patch and the ground plane. The max $F(\theta, \phi)$ should be normal to the patch i.e. a broadside radiator. The general approximation of the range of length in which the patch is resonant is $\lambda_0/3 < L < \lambda_0/2$. The substrate to be chosen normally comes from a big selection from several different manufacturers and has a dielectric constant between $2.2 \leq \epsilon_r \leq 12$ [11].

4.1 Choosing a Substrate

This choice, in reality, is a compromise between good antenna performance and microwave circuitry design one has to settle for. Using a thin substrate with a dielectric constant that is on the higher end of the above-mentioned range is preferable for microwave circuit designing as such designing often needs tightly bound fields to minimize mutual coupling and unwanted radiation. This choice gives us a smaller element size but at the expense of efficiency and bandwidth. On the other hand, selecting a thick substrate with a dielectric constant that is on the lower end of the above-mentioned range is preferable when the only aspect of judging the design is the antenna performance. Loosely bound fields help radiate effectively into space making efficiency and bandwidth greater but at the expense of a larger element size. In this project, we have chosen Rogers RO4350B while designing the TX part and FR-4 while designing the RX part.

4.2 Calculating the Dimensions

The rectangular patch is L long and W wide. The input reactance of the patch becomes zero i.e. it becomes resonant when the length is kept at half a wavelength in the dielectric and is then known as the half-wave rectangular patch. In reality, as L and W are not infinite, there is fringing in the fields at the edges of the patch which makes the effective length more than its physical length disturbing the resonant frequency as the resonant length now would be less than half a wavelength. The extent of this fringing effect depends on the length and width of the microstrip

patch as well as the height of the substrate. To start off, a good approximation of the length and width can be made by the following formulae:

$$L \approx 0.49\lambda_d = 0.49\frac{\lambda}{\sqrt{\epsilon_r}} \tag{4.1}$$

$$W = \frac{\lambda}{\sqrt{\epsilon_r}} \tag{4.2}$$

After this we have to calculate the input impedance as a function of frequency, for this we use:

$$Z = 90\frac{\epsilon_r^2}{\epsilon_r - 1}\left(\frac{L}{W}\right)^2 \tag{4.3}$$

This value ranges from a 100 to 400 Ω. Now we can scale the model in size to shift the resonance frequency to the desired design frequency as the formulas mentioned above are approximate analytical models designed in the early years of Micro Strip patch Antennas for input impedance, radiation pattern and bandwidth calculations but they are, still to this date, used as a first step in computer simulations because of their ability to yield formulas containing empirically based parameters. More recent advancements, however, have given two more accurate and now widely used analytical models, namely, the transmission line and the cavity model. The interested reader is referred to H.6: Balanis, 3rd ed., Chap 14. The design formulas presented in these start off with a more accurate resonant microstrip patch length:

$$L = 0.5\frac{\lambda}{\sqrt{\epsilon_r}} - 2\Delta L \tag{4.4}$$

Where

$$\frac{\Delta L}{h} = 0.412\frac{(\epsilon_{reff} + 0.3)\left(\frac{W}{h} + 0.264\right)}{(\epsilon_{reff} - 0.258)\left(\frac{W}{h} + 0.8\right)} \tag{4.5}$$

ΔL is called the fringing length, which is an extension (not physical) to the actual length of the patch on each end and is a function of the width to height ratio and the effective dielectric constant. Most of the electric field lines travel in the substrate but some of them also travel in air, hence the effective dielectric constant. It is also a function of the resonant frequency in such a way that as the frequency of operation goes up, the effective dielectric constant approaches the actual dielectric constant as this means most of the electric field lines are now concentrated in the substrate. It is given by:

$$\epsilon_{reff} = \frac{\epsilon_r + 1}{2} + \frac{\epsilon_r - 1}{2}\left[1 + 12\frac{h}{W}\right]^{-1/2} \tag{4.6}$$

For the case where achieving the desired input impedance is the goal the formula to calculate the accurate width is given by back solving the following:

$$Z_A = 90\frac{\epsilon_r^2}{\epsilon_r - 1}\left(\frac{L}{W}\right)^2 \tag{4.7}$$

$$i.e. W = \frac{90L}{\sqrt{Z_A}}\frac{\epsilon_r^2}{\epsilon_r - 1} \tag{4.8}$$

For the case where high efficiency is the goal, which in our case is, the patch width is provided by

$$W = \frac{\lambda}{2}\left[\frac{\epsilon_r + 1}{2}\right]^{-1/2} \tag{4.9}$$

It should be remembered here that the length should be recalculated to get more accurate results.

4.3 Choosing a feeding method

There are many different techniques to feed a microstrip patch, among which the four most widely used are the microstrip line feed (edge and inset), probe feed, proximity coupled feed and the aperture coupled feed. For building microstrip arrays though, where planar and low-profile realizations are the goal, the microstrip line is the best-suited feeding technique which gives the possibility to fabricate the patch, feed network and other network components on a single layer. The difficulty with the simplified microstrip line edge feed technique arises when the input impedance needs to be controlled where the only means of doing so is by changing the dimensions of the patch. To solve such an issue, a quarter wave transformer is used which gives another degree of freedom to control the input impedance.

A quarter wavelength transformer (see Fig. 4.2) is basically a transmission line of a quarter the wavelength that is used to match the input impedance of the patch to the characteristic impedance of the transmission line which is usually 50Ω (see Fig. 4.3). The characteristic impedance of this quarter wavelength transformer is then given by

$$Z_{qwt} = \sqrt{Z_A Z_0} \qquad \text{(Impedances are real valued)} \tag{4.10}$$

A microstrip line's characteristic impedance is dependent on its width i.e. the wider the microstrip line the lower the characteristic impedance.

In designing a microstrip patch array, however, which is our ultimate goal for this project, the microstrip edge feed technique which combines the quarter wavelength transformer with an inset distance (see Fig. 4.1) gives the designer two

degrees of freedom to control the input impedance, where the extra degree of freedom comes from varying the inset distance. It should be kept in mind that this is not a suitable feeding network scheme when the substrate used is of very high permittivity as this would mean a very large inset depth must be used which will obviously affect the radiation pattern.

The two-layer design can always be used when building the array where the top layer houses the patches and the bottom layer can house the microstrip feed network but the challenge was always to do it in the same layer and it was achieved as will be clear further on.

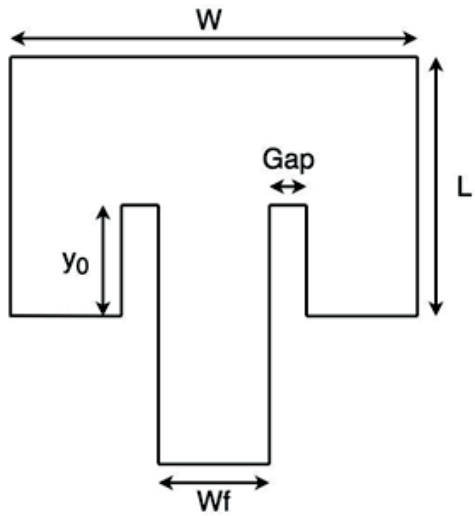

Figure 4.1: Model of micro strip line inset fed patch antenna

The inset distance is calculated by the following formulae [12]:

$$y_0 = \frac{L}{\pi} cos^{-1}\left(\sqrt{\frac{Z_{in}}{R_{in}}}\right) \tag{4.11}$$

$$Y_0 = 10^{-4}\left\{\begin{array}{l} 0.001699\epsilon_r^7 + 0.13761\epsilon_r^6 - 6.1783\epsilon_r^5 + 93.187\epsilon_r^4 \\ -682.69\epsilon_r^3 + 2561.9\epsilon_r^2 - 4043\epsilon_r + 6697 \end{array}\right\}\frac{L}{2} \tag{4.12}$$

Where although the second equation was found to be much more accurate and gave the best simulation results, it is only valid for $2 \leq \epsilon_r \leq 10$.

The width of the micro strip line feed is given by back solving the following equation with the characteristic impedance Z_c of the micro strip line feed set as 50Ω:

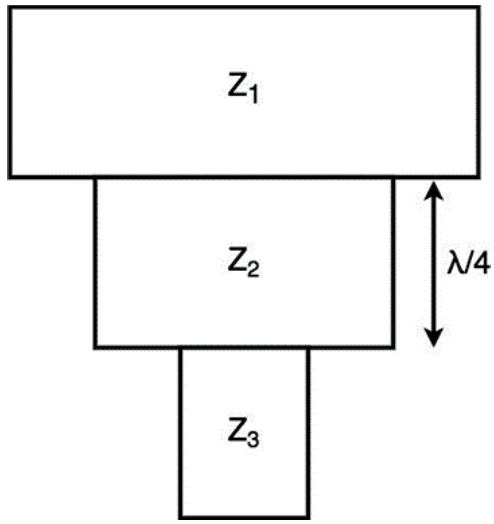

Figure 4.2: Model of a basic quarter wave transformer

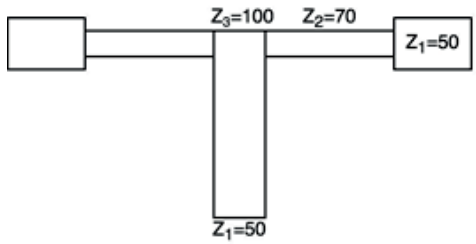

Figure 4.3: Quarter wave transformer when used to match the patch to the 50 Ω feed

$$Z_c = \begin{cases} \frac{60}{\sqrt{\epsilon_{reff}}} \ln[\frac{8h}{W_0} + \frac{W_0}{4h}], & \frac{W_0}{h} \leq 1 \\ \frac{120\pi}{\sqrt{\epsilon_{reff}}[\frac{W_0}{h} + 1.393 + 0.667 \ln(\frac{W_0}{h} + 1.444)]}, & \frac{W_0}{h} > 1 \end{cases} \tag{4.13}$$

4.4 Simulation

From the discussion above, the patch was designed on the latest version of CST i.e. CST Studio Suite 2018 using the modeling tools provided in the CST MW studio. The model itself (see Fig. 4.4) and the results it produced are given below:

In order to optimize the patch dimensions obtained from the theoretical results, a comprehensive study was done as to which of the parameters affect the two most important results for any antenna design i.e. the resonant frequency and the return

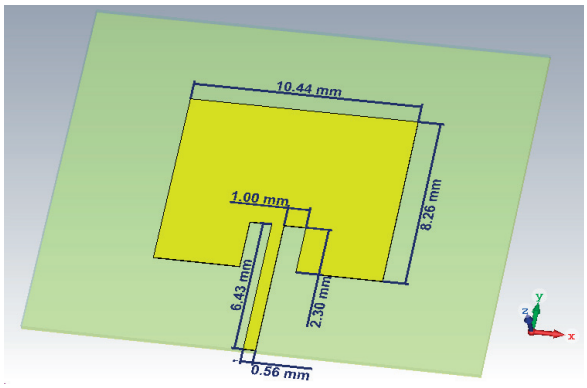

Figure 4.4: Designed patch antenna with the optimized dimensions

loss. The two parameters turned out to be the length of the patch and the inset distance which were then fine-tuned with the resulting graphical representations shown in Figs. 4.5 and 4.6, summarized in Tables 4.1 and 4.2.:

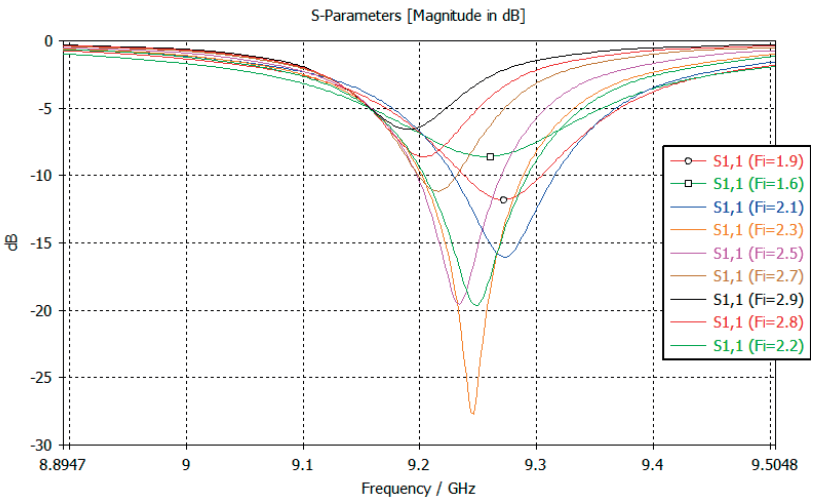

Figure 4.5: Studying the inset depth Fi with operating frequency set at 9.41 GHz, patch width set at 10.443mm, patch length set at 8.42mm, the substrate height set at 0.254mm, the thickness of the copper set at 0.035mm, the width of the micro strip feed set at 0.56 mm

4.5 Optimization

From the two sets of figures and tables above, it can be seen that the inset distance Fi has much greater influence on the reflection coefficient S1,1. When inset depth

Fi (mm)	S1,1(dB)	VSWR	Freq(GHz)	Gain(dB)	Directivity (dB)
1.9	-11.7924	1.6927	9.2710	5.99	7.24
2.0	-13.5539	1.5318	9.2725	5.97	7.24
2.1	-16.0387	1.3767	9.2725	5.94	7.24
2.2	-19.6480	1.2324	9.2485	5.80	7.24
2.3	-27.7720	1.0852	9.2455	5.75	7.24
2.4	-29.6543	1.0680	9.2410	5.67	7.23
2.5	-19.5658	1.2349	9.2335	5.69	7.23
2.6	-14.5200	1.4628	9.2245	5.71	7.22
2.7	-11.1570	1.7654	9.2155	5.67	7.22

Table 4.1: The corresponding table confirming the results

L(mm)	S1,1(dB)	VSWR	Freq(GHz)	Gain(dB)	Diretivity(dB)
8.22	-30.1977	1.0638	9.452	5.96	7.22
8.23	-31.3306	1.0558	9.440	5.96	7.22
8.24	-32.7966	1.0470	9.430	5.94	7.22
8.25	-34.2327	1.0396	9.420	5.94	7.22
8.26	-35.3837	1.0346	9.410	5.94	7.22
8.27	-38.4948	1.0240	9.398	5.94	7.22
8.28	-42.2220	1.0156	9.388	5.95	7.23
8.29	-44.7108	1.0117	9.378	5.97	7.23
8.30	-43.0752	1.0141	9.368	5.98	7.23

Table 4.2: The corresponding table confirming the results

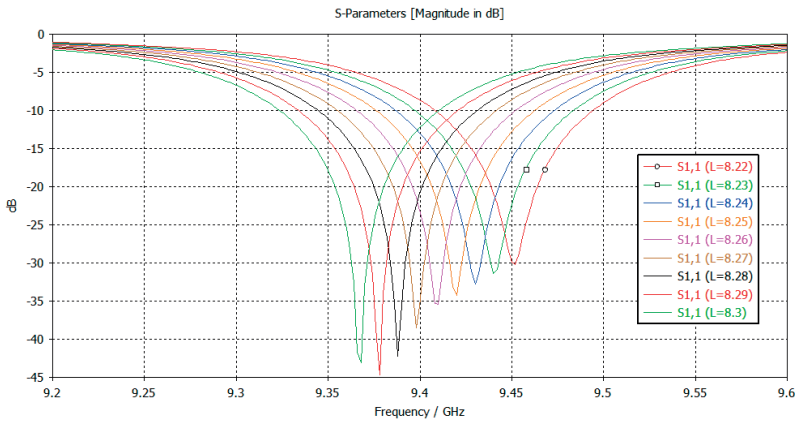

Figure 4.6: Studying the length L with operating frequency set at 9.41 GHz, patch width set at 10.443mm, inset depth set at 2.3mm, the substrate height set at 0.254mm, the thickness of the copper set at 0.035mm, the width of the micro strip feed set at 0.56 mm

is increased, the shift in the resonant frequency is both rapid and random. However, when the length L of the patch is increased, both the reflection coefficient and the resonant frequency change, but in a more stable and predictable manner.

In a case like this the best approach is as follows:

- Design and simulate a single patch antenna with the dimensions obtained from the formulae mentioned earlier in the report.
- Find an ideal inset depth Fi to get the best possible result in terms of reflection coefficient S1,1 i.e. the least possible, where the general rule of thumb is that as you decrease the inset depth the S1,1 results get better but there is however a sharp convergence point after which the case is reversed.
- Then, finally, keep changing L to move the resonant frequency to the desired value, here, the general rule of thumb is that as you increase the patch length L, the resonant frequency will drop i.e. the frequency at which your antenna is operating will get lower and vice versa.

The gap shown in Fig.4.5 is generally set at 1mm in almost every study of a micro strip patch antenna with an inset version of the micro strip line feed.

This comprehensive behavioral study lead to optimum like simulation results where the final set of data used to simulate the patch was as follows:

- Length of the patch = 8.26 mm
- Width of the patch = 10.443 mm
- Inset Depth = 2.3 mm

- Feed Width = 0.56 mm
- Substrate Thickness = 0.254 mm
- Copper Thickness = 0.035 mm
- Inset Gap = 1 mm

The substrate used was from Rogers Corporation from their RO4000 series, model RO4350B, which has a dielectric constant of 3.66. The simulation results including the S1,1 parameter, VSWR, 2D/3D far-field gain and 2D/3D far-field directivity are shown in Figs. 4.7-4.12.:

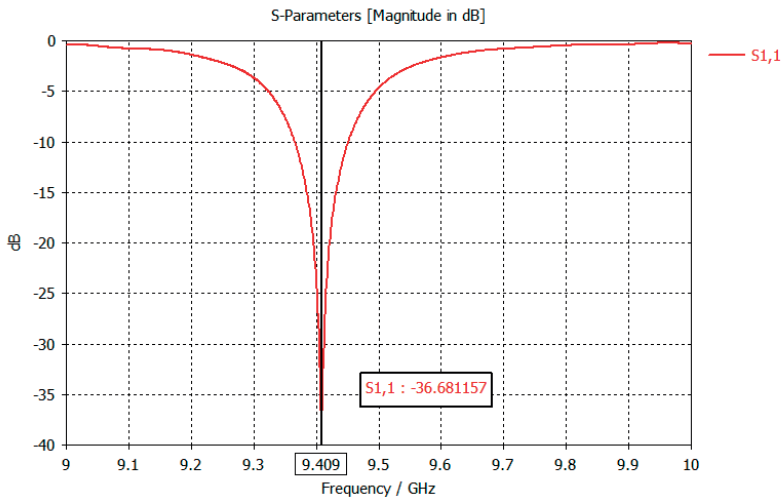

Figure 4.7: Reflection coefficient S1,1 of approximately -37 dB achieved at 9.41 GHz

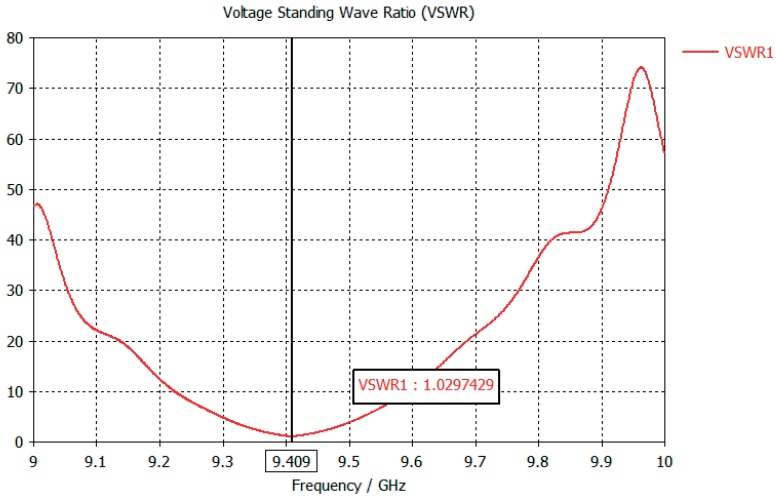

Figure 4.8: Voltage standing wave ratio VSWR of 1.0297 achieved at 9.41 GHz

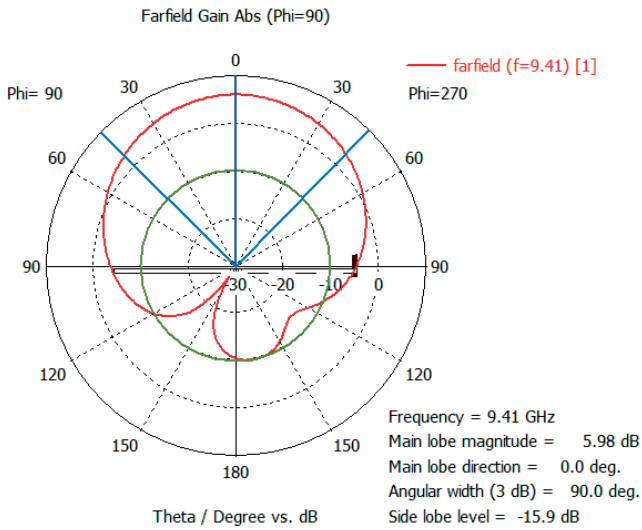

Figure 4.9: Polar plot of Far field Gain of approximately 6dB achieved for the single patch with 90deg angular beam width

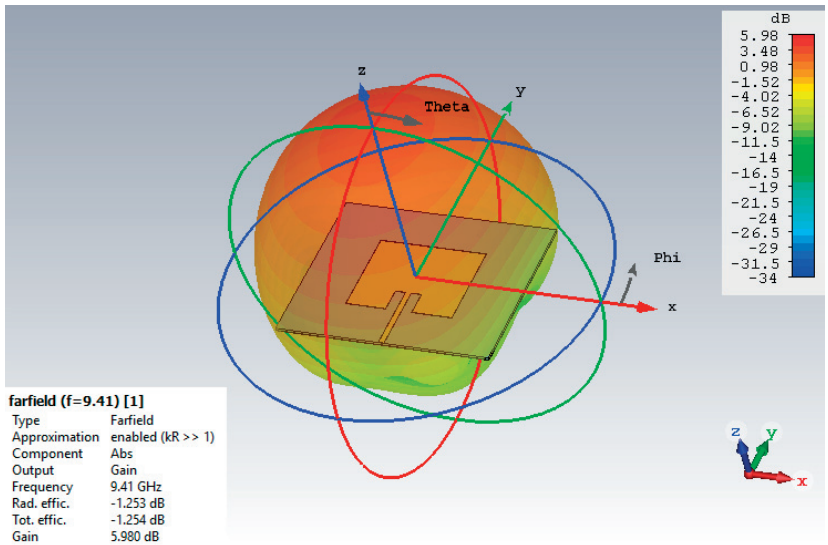

Figure 4.10: Far field gain 3-D plot showing total efficiency of approximately 75% (-1.254 dB)

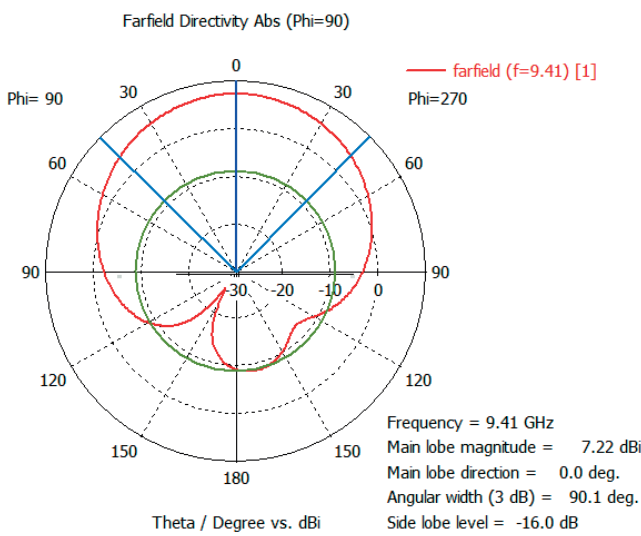

Figure 4.11: Polar plot of Far field directivity of 7.23dB achieved for single patch with 90° angular beam width

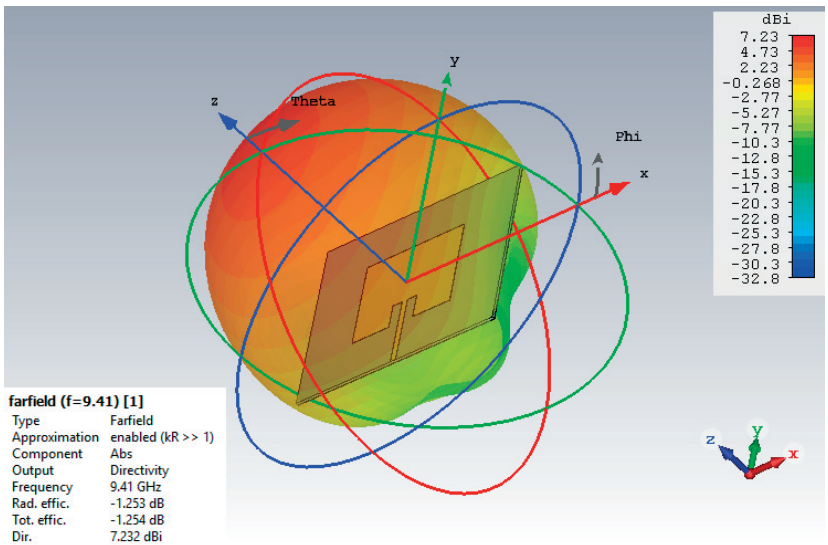

Figure 4.12: Far field directivity 3-D plot showing total efficiency of approximately 75% (-1.254dB)

Chapter 5

Building an Array & Choosing the Feed Network

A single element microstrip patch antenna can never achieve a gain of more than 10dB no matter which way we design it, but in many scenarios such as the one we are trying to explore, where the low profile nature has to be combined with moderate to high gain the only attractive solution is to design an array of microstrip patch antennas. For fixed phase microstrip patch arrays there are two main things that need to be kept in mind during the design process, the inter-element spacing (the distance between two adjacent patch antennas) and the type of feed network (relative orientation and separation of patch antennas) used because this leads to the phenomenon of mutual coupling. In a real array, all the participating elements interact with each other, which results in the altercation of currents which consequently alters the impedances. This altercation, called the mutual coupling changes the current magnitude, phase and distribution on each element from their free space values. This results in the radiation pattern of the array to be unsymmetrical and is most usually a function of the position of one patch element relative to the other. It can be attributed to the various fields that exist along the air-dielectric interface such as the space waves, higher order waves, surface waves and leaky waves. The former two contribute the most when the inter-element spacing is small because they radiate in a spherical manner. There are three classical array configurations, namely, the side by side, the collinear and the parallel in echelon. The side by side configuration exhibits the largest variation in the mutual impedance and is a function of the relative alignment of the elements. When positioned collinearly along the E-plane, the coupling is smallest for small spacing i.e. $s < 0.10\lambda_0$ and when positioned collinearly along the H-plane, the coupling is the smallest for large spacing i.e. $s > 0.10\lambda_0$. The general rules of thumb when assessing mutual coupling in microstrip arrays are as follows [H.6: Rudge et al., Vol. II, Sec. 10.3]:

- The magnitude of mutual impedance decreases with inter element spacing distance and in most cases decaying as $\frac{1}{s^2}$.[H.8.2: Hansen, "Phased Array Antennas", 2nd ed., p. 225].

- Elements with a narrow radiation pattern will have lower coupling than elements with a broad radiation pattern

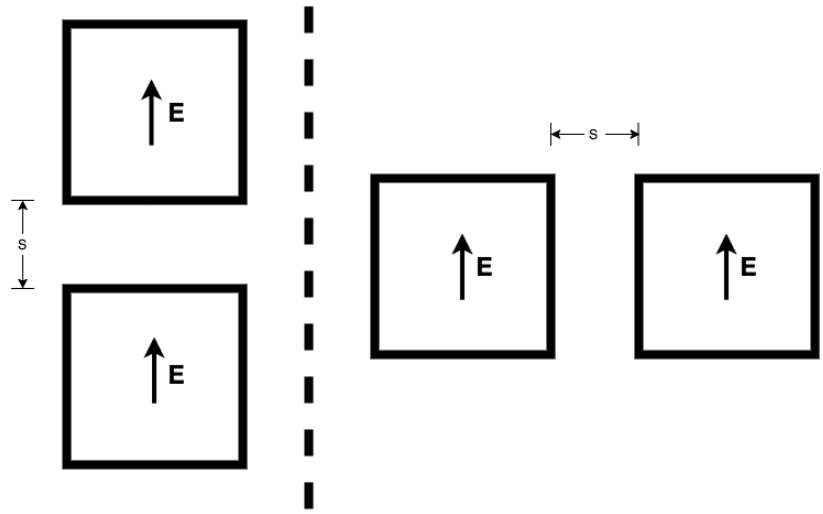

Figure 5.1: E and H plane arrangements of the micro strip patch elements [11]

- Elements with parallel polarizations couple more than collinear polarization ones.
- Larger elements have smaller coupling.

It is also seen that mutual coupling may not be encountered in arrays where patch elements are spaced $0.57\lambda_0$ apart.

The feeding network can consist of a single line or it can consist of multiple lines in a network like an arrangement. The former is known as series-feed network shown in Fig. 5.2 and the latter is known as a corporate-feed network shown in Fig. 5.3. Series-feed networks are easy to fabricate for both the radiating elements and the feed network. Any changes in one of the elements or the feed lines though mean the performance of the others. This kind of feeding technique can also only be applied to fixed beam arrays but it is, however, more compact. Corporate-feed networks are more commonly used because of their versatility. This kind of network has equal path lengths to each radiating element which gives wider bandwidth than series-fed networks. Although the successive branches used in a corporate-fed network lower the input impedance; proper impedance can be maintained by using micro strip transmission lines which enables impedance matching, phase control and amplitude tapering, all on a single layer which is a major advantage over the other feeding implementations. A quarter wave transformer mentioned in the previous chapter helps in achieving this by matching the impedance. This impedance matching pattern is repeated as sub arrays are added to build even larger arrays. It must also be noted that as the number of elements in the array increases, so does the surface wave losses, dielectric losses, connector losses and conductor losses and it is considered as the main goal to control these losses when building an array

with the highest possible gain. In other words, the efficiency of the micro strip array will drop as we increase the number of elements.

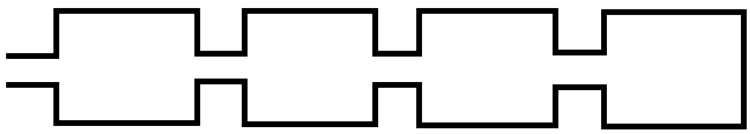

Figure 5.2: The series-feed network

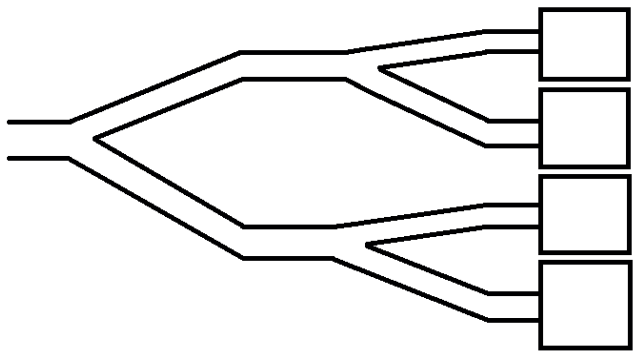

Figure 5.3: The corporate-feed network

Taking into account all this knowledge, a simple 2 x 4 array was designed with the same dimensions as in the previous chapter for the single patchwith the CST model shown in Fig. 5.4 and the S1,1, VSWR and 2D/3D far field gain results shown in Figs. 5.5-5.10.

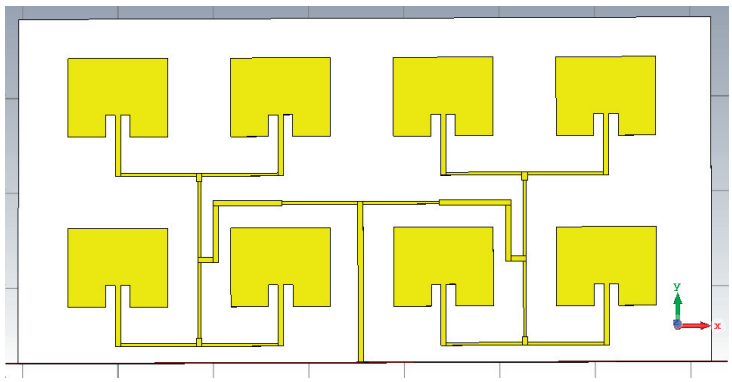

Figure 5.4: CST design model for the 2 x 4 array

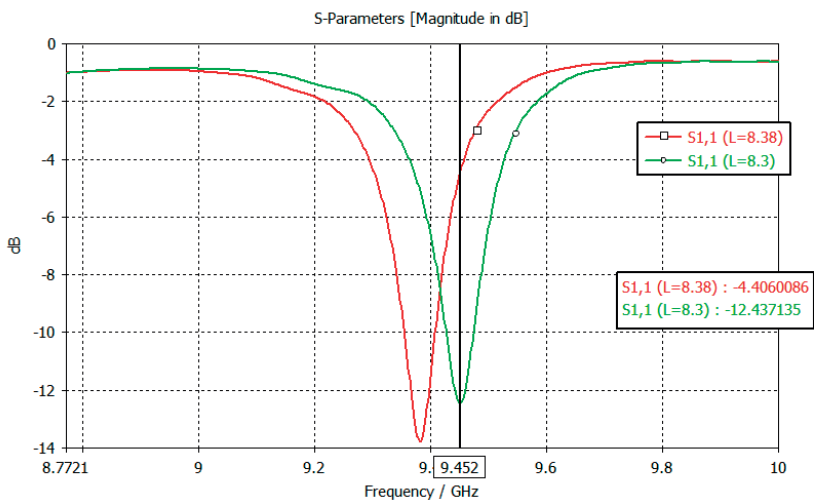

Figure 5.5: Suboptimal Reflection coefficient S1,1 of approximately -11 dB achieved at 9.41 GHz during the first attempt at designing corporate feed network

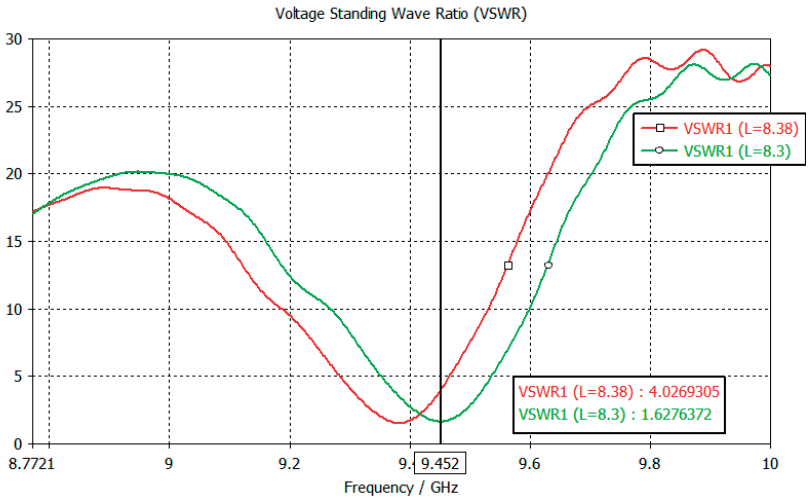

Figure 5.6: Suboptimal Voltage standing wave ratio VSWR of just under 2 achieved at 9.41 GHz

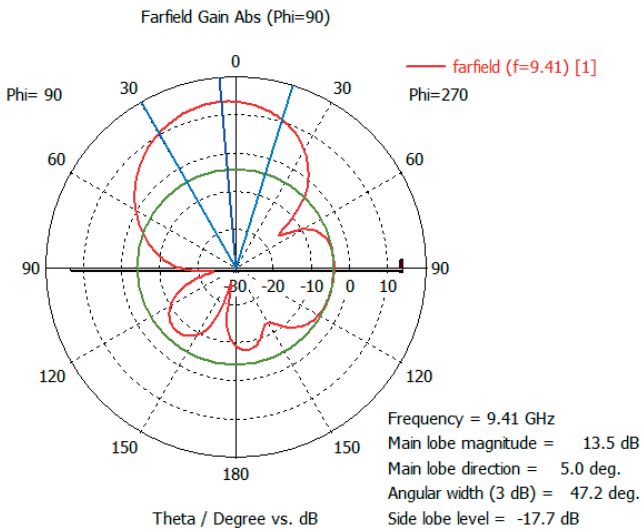

Figure 5.7: Polar Plot of Far field Gain of 13.5 dB at 9.41 GHz with an angular beam width of 47°

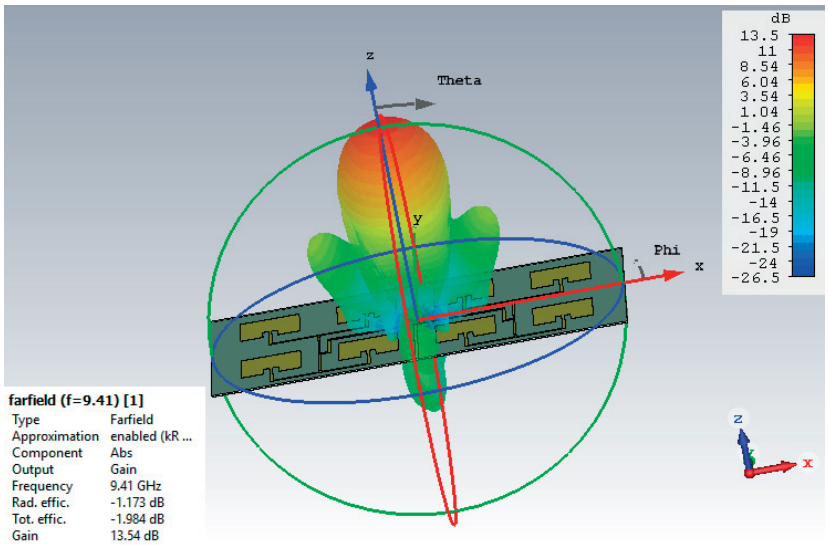

Figure 5.8: Far field gain 3-D plot with total efficiency of only 64% (-1.984 dB)

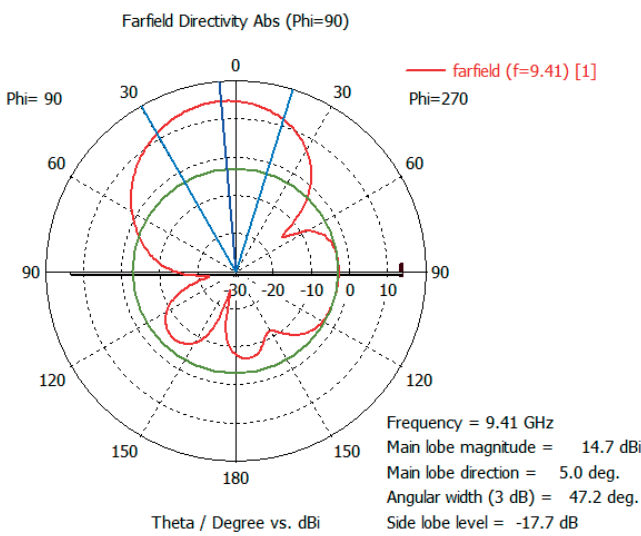

Figure 5.9: Polar plot of Far field directivity of 14.7 dB at 9.41 GHz with an angular beam width of 47°

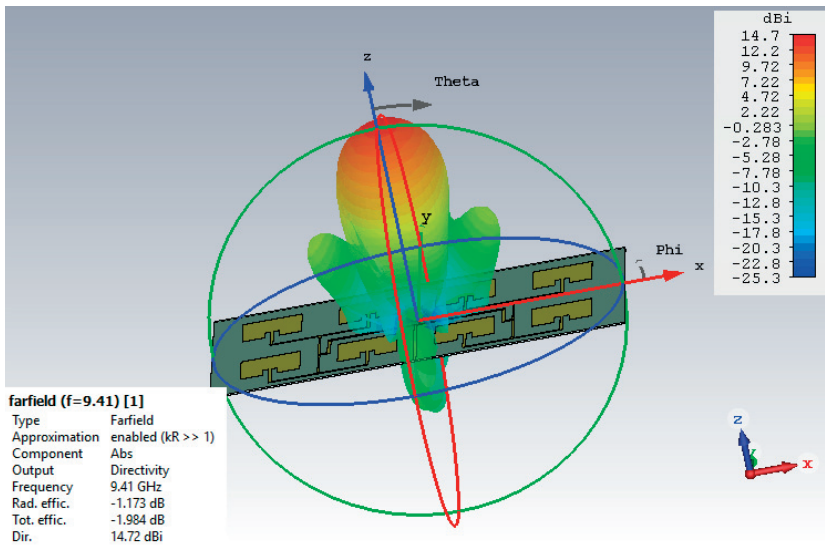

Figure 5.10: Far field directivity 3-D plot with total efficiency of only 64% (-1.984dB)

Chapter 6

Designing the TX Micro Strip Patch Array

6.1 Configuration

For the TX array, we tried two configurations, firstly a 4 x 8 multiple antenna system. The inter-element spacing for fixed beam arrays should always be less than a wavelength (λ) to avoid grating lobes which usually occur in uniformly spaced arrays (arrays with radiating elements equidistant from each other) [9] and it should be kept greater than half a wavelength (λ /2) so that we have enough room for the design of the feeding network which aims at suppressing the mutual coupling and providing higher gain as a result. After careful consideration, this value was chosen to be a little higher than half a wavelength at 0.5351λ i.e. $2xW_f{+}0.5x\lambda$ which is equal to 17.06 mm.

6.2 Impedance Matching

The feeding technique used is a parallel network i.e. corporate feed and the patch elements were matched to the 50 Ω input using a quarter wave transformer. This matching can be made successful when the characteristic impedance of the quarter wavelength transformer $Z_{qwt} = \sqrt{Z_1 Z_2}$. A transmission line that is of length 0.25λ is used for the purpose, hence the name where $\lambda = \lambda_0 \ /\epsilon_{reff}$. In theory, it provides a perfect match with no reflection at the desired operating frequency. The width of this matching line has to found via an iterative method where we use $Z_0 = \frac{60}{\sqrt{\epsilon_{reff}}} \ln\left[\frac{8h}{W_0} + \frac{W_0}{4h}\right]$,if $\frac{W}{h} < 1$, and change the width until Z_0 matches Z_{qwt}.

It must be noted that the lines with higher impedances will always have a smaller width as compared to the lower impedance lines.

6.3 Simulations

The theoretical dimensions calculated from the formulae found in literature provided a very good estimate of what was required to achieve good results in terms

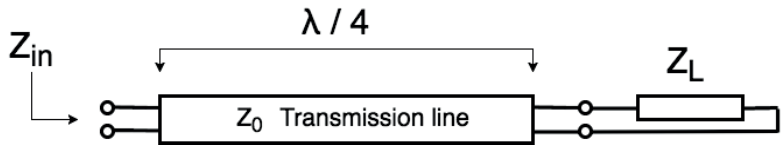

Figure 6.1: A quarter-wave transmission line [18]

of resonance, array gain, beam width and VSWR but some tweaking had to be done in order to introduce perfection into the simulated designs. The graphical representations of the S1, 1 parameter (return loss), VSWR and the 2-D/3-D plots of the array gain are given in Figs. 6.2-6.8 along with the array configuration:

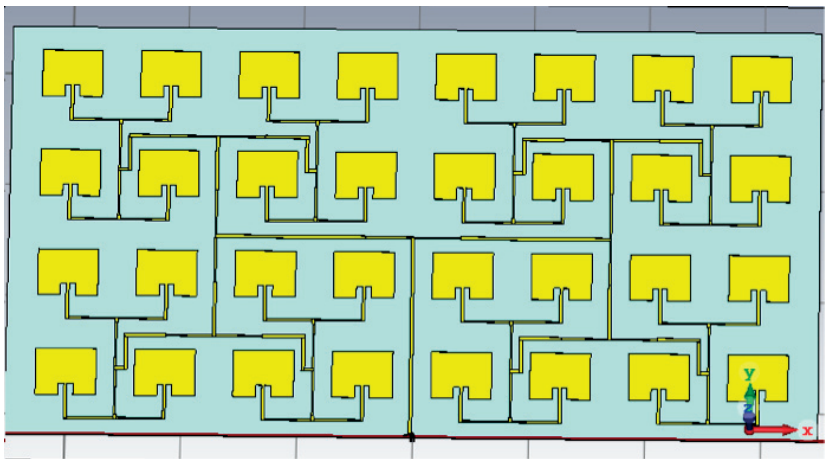

Figure 6.2: Initial 4x8 array configuration with corporate feed using quarter wave transformers.

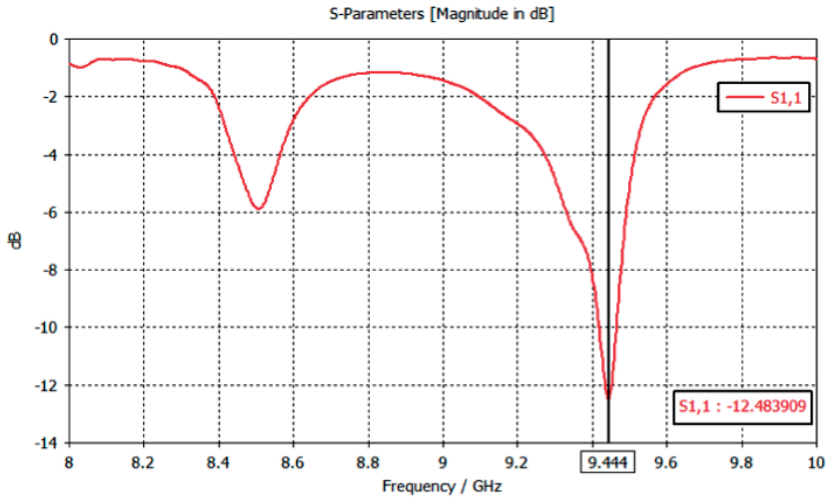

Figure 6.3: The S1, 1 parameter plot showing the array is resonant at around approximately 9.41 GHz.

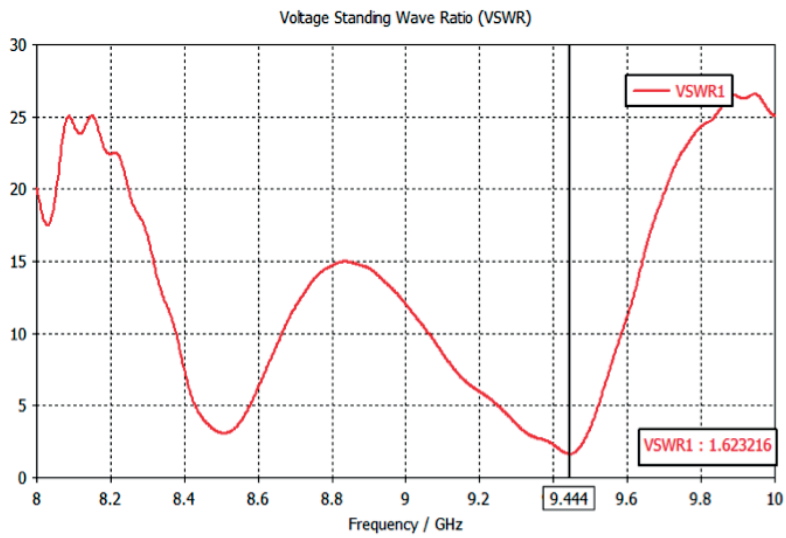

Figure 6.4: VSWR plot showing it to be less than 2.

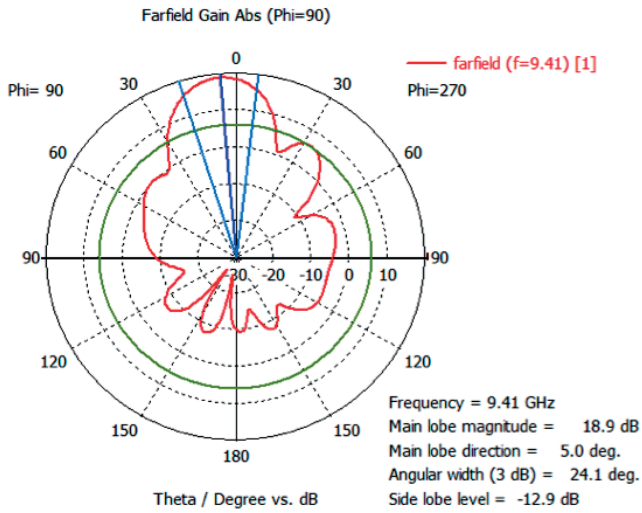

Figure 6.5: 2-D far-field gain plot with a main lobe magnitude of approximately 19 dB and an angular beam width of 24.1°.

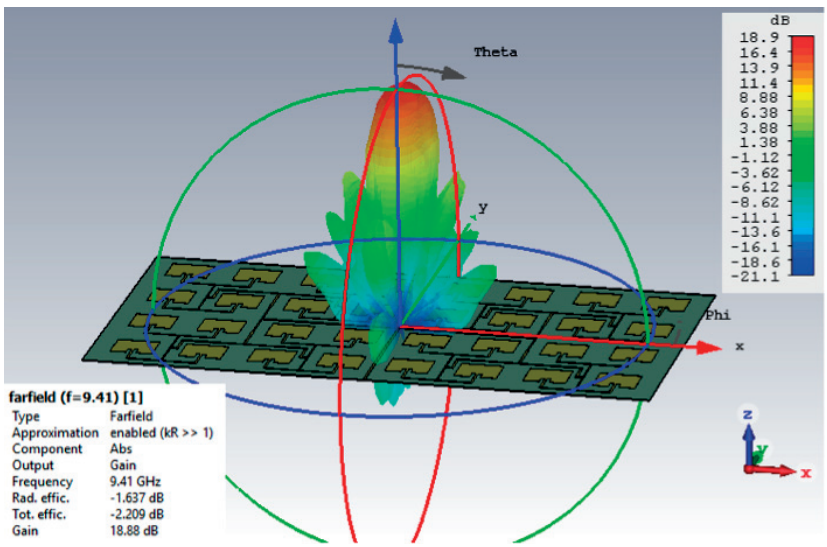

Figure 6.6: 3-D far-field gain plot showing the radiation efficiency of approximately 69% (-1.637dB)

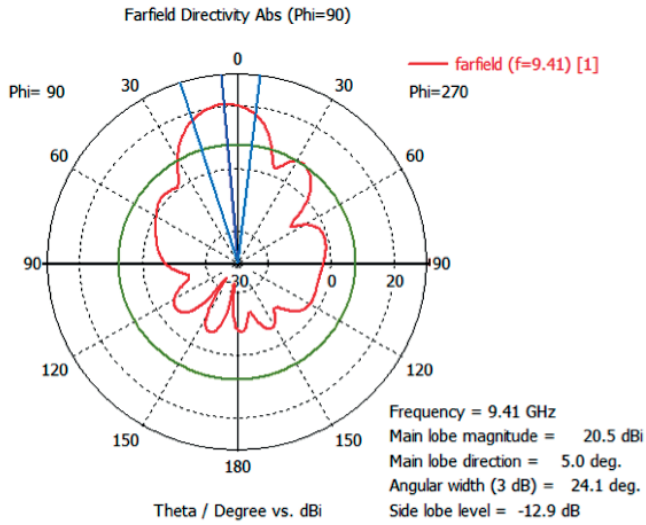

Figure 6.7: 2-D far-field directivity plot with a main lobe magnitude of approximately 20.5 dB and an angular beam width of 24.1°.

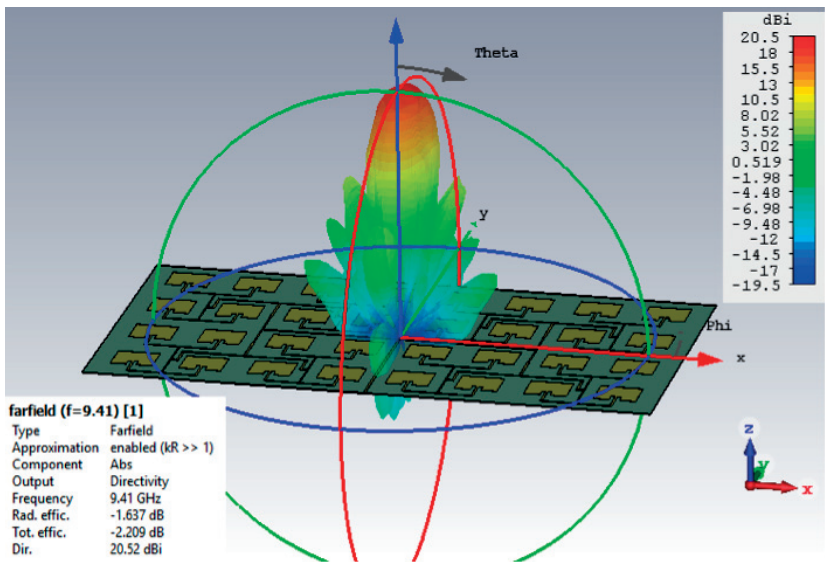

Figure 6.8: 3-D far-field directivity plot showing the radiation efficiency of approximately 69% (-1.637dB)

Chapter 7

Designing the RX Micro Strip Patch Array

7.1 Array Parameters & Challenges

The main goal of this project as should be clear from the title itself was to make both the RX and TX arrays as compact as possible while keeping the performance as high as possible. It was a challenge to deliver an array gain of well over 20dBi while maintaining the low profile nature and cost. The upper limits on the dimensions were 210 x 210 mm (± 10 mm) whereas the actual designed arrays came out to be at a combined 220 x 145 mm. The maximum possible number of radiating elements that we could accommodate in such restrictions were 128 for the RX array and 64 for the TX array. Before the final geometry and numbers were decided though, it was not known what the beam widths would be for the two different patch antenna arrays. For the radar system to work efficiently it is essential to match the beam widths because assuming constant transmitted power, decreasing the beam width will result in a higher gain antenna main beam. This decrease in beam width means that fewer interferers will have significant effect on the typical receiver but their individual effects will be stronger. Additionally, as the beam width is decreased, the proper alignment of the TX and Rx arrays becomes much more difficult, but when matching is achieved, the desired signal strength is increased significantly, in other words, the transmit power is used in an efficient manner. Keeping the discussion in Section 5 in mind, the same technique was used to build the RX array. The 4 x 8 TX array was redesigned for the new resonant frequency i.e. the second harmonic of the fundamental frequency 9.41 GHz which is 2 x 9.41 GHz = 18.82 GHz.

Using the same set of equations in Section 4, the RX patch antenna dimensions were calculated to be as follows with the CST model shown in Fig. 7.1.:

- Length of the patch = 3.888 mm
- Width of the patch = 5.2215 mm
- Inset Depth = 0.9 mm
- W_f = 0.498 mm
- Substrate Thickness = 0.254 mm
- Copper Thickness = 0.035 mm

- Inset Gap = 1 mm

The inter element spacing in the case of the RX array was chosen to be a fraction greater from the case of the TX array at 0.5627λ i.e. $(2\times W_f\ )+(0.5\times\lambda)$ which is 8.97 mm.

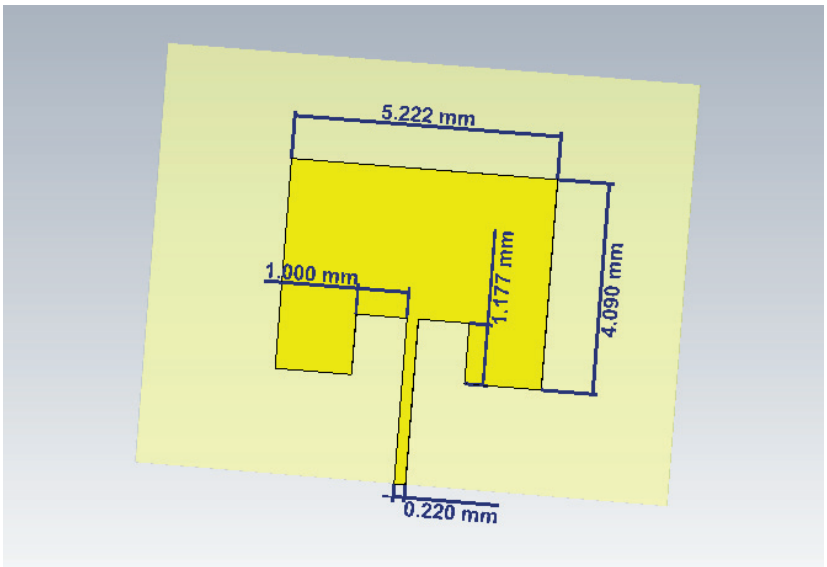

Figure 7.1: CST model for the patch antenna designed to be resonant at 18.82 GHz along with its dimensions

7.2 Effects of the Substrate Properties

The substrate used in this case was first the same i.e. Roger RO4350B but then changed FR-4 and the reason for choosing the height to be 0.254 mm is because it had more good consequences than bad ones. It is a trade off which every antenna designer faces i.e. to either use a thinner substrate with low dielectric constant or a thicker substrate with high dielectric constant. There seems to be a consensus in the previous literature over the point that lower dielectric constant substrates usually improve the overall efficiency of a patch antenna when the thickness is kept the same but that is not true in the case when working with microwave circuitry. Generally, if the dielectric constant is higher, the electric fields are more tightly contained inside the substrate which results in less radiation but in micro wave circuitry it is a means to minimize undesired radiation and mutual coupling. A low dielectric constant substrate will increase the fringing field at the patch periphery and thus the radiated power. According to the discussion in Section 4, if the substrate chosen is the Roger TMM 10 which has a dielectric constant of 9.8, it will greatly decrease the patch size which would mean we could fit in more radiating elements and increase the performance but that is not the case as just discussed above and the performance degrades. There is not just one aspect to

think about because the height/thickness of the substrate also plays a vital role in overall performance. A thicker substrate, besides being mechanically strong, will increase the bandwidth, radiated power and conduction efficiency but the resonant frequency will decrease and the antenna pattern and polarization will degrade through dielectric losses (decrease in dielectric efficiency), surface wave losses and extraneous radiations. A general rule of thumb for the limit on the height/thickness of the substrate is as follows:

$$0.003\lambda_0 \leq h \leq 0.05\lambda_0 \tag{7.1}$$

An increase in the thickness of the substrate, thus, has a similar effect on antenna characteristics as a decrease in the value of the dielectric constant. A high loss tangent will increase the dielectric losses and therefore reduce antenna efficiency. To make it easier to understand, there is no ideal substrate; rather the choice depends on the application.

Using the discussion in Sections 4 and 6, We can find out the width of the micro strip line feed and the quarter wave transformer which will be used for impedance matching of the patch elements and the 50 Ω input line.

The same parallel network as in Section 6 i.e. the corporate feed was used and the following 8x16 RX array was designed as shown in Fig. 7.3.

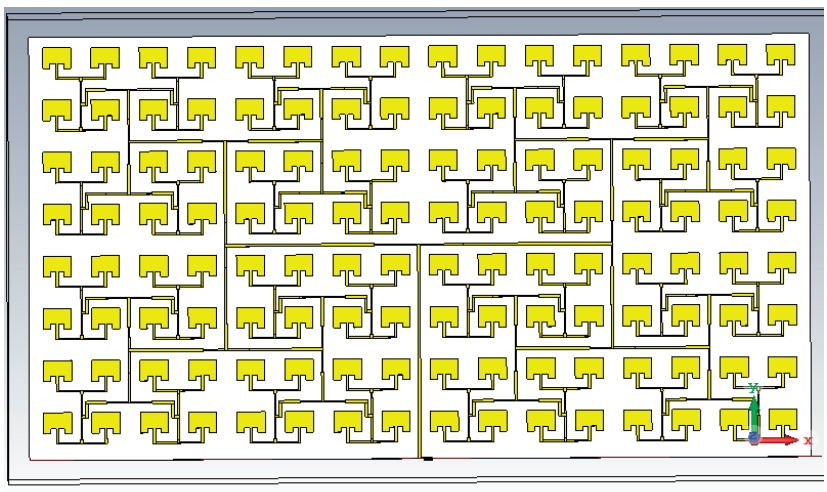

Figure 7.2: CST design model for the final 8x16 RX array with corporate feed using quarter wave transformers

Appropriate adjustments were made to the patch dimensions after some investigation to reduce the coupling effect and optimize the results. The substrate finally chosen was FR-4 due to its slightly higher dielectric constant and consequently the ability to contain the electric fields tightly and minimize undesired radiation and mutual coupling which would otherwise be much stronger and degrade the

performance due to having four times the number of radiating elements compared to the TX array case. The simulation results are shown in Figs. 7.4-7.9.:

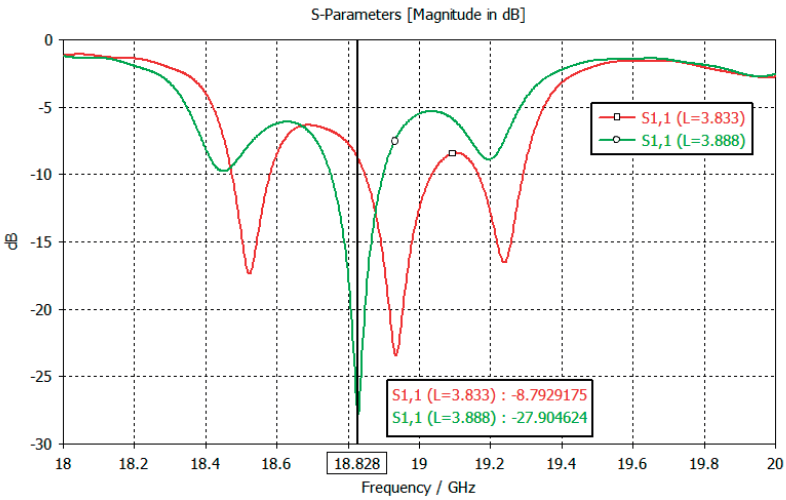

Figure 7.3: Reflection coefficient S1,1 of approximately -28 dB achieved at 18.82 GHz

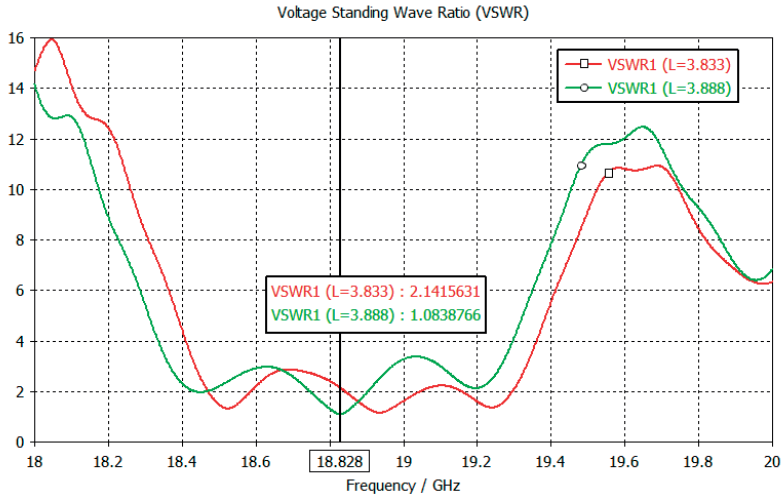

Figure 7.4: Voltage standing wave ratio VSWR of 1.0838 achieved at 18.82 GHz

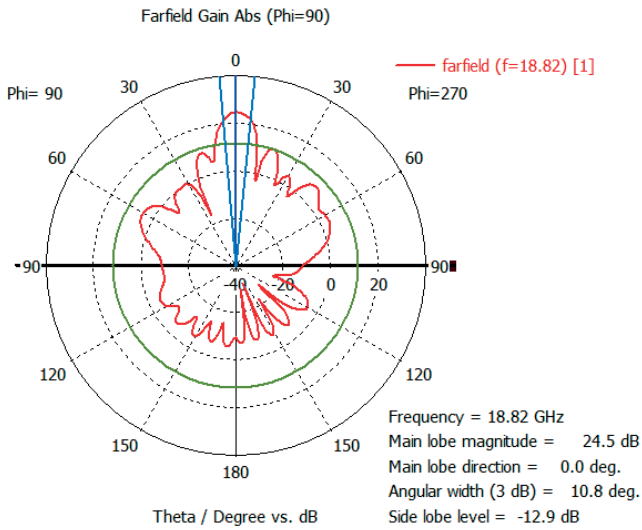

Figure 7.5: Polar Plot of Far field Gain of approximately 25 dB at 18.82 GHz with an angular beam width of 10.8°.

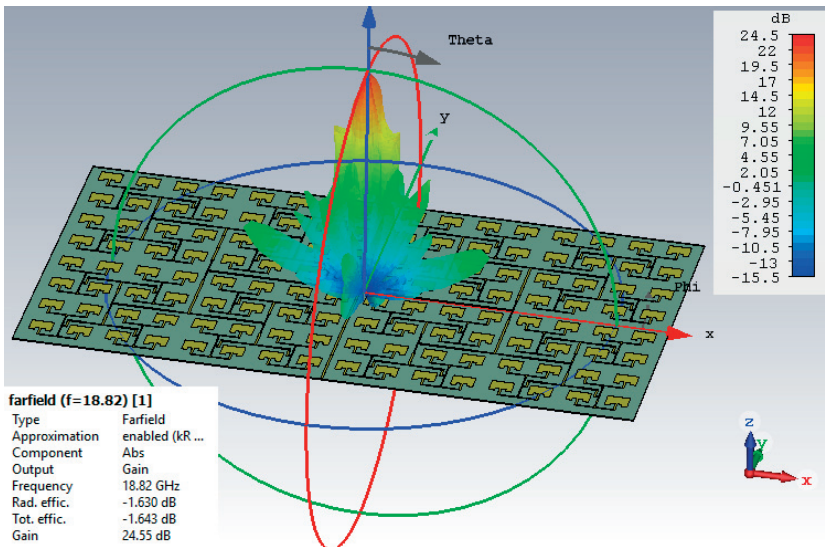

Figure 7.6: Far field gain 3-D plot with total efficiency of around 70% (-1.63 dB)

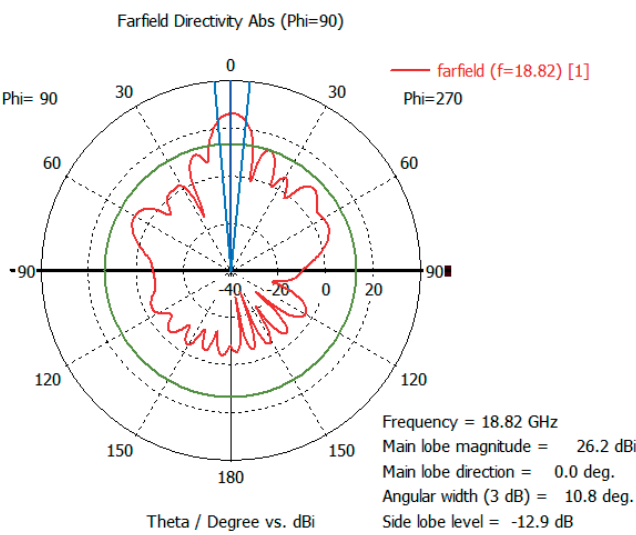

Figure 7.7: Polar plot of Far field directivity of 26 dB at 18.82 GHz with an angular beam width of 10.8°.

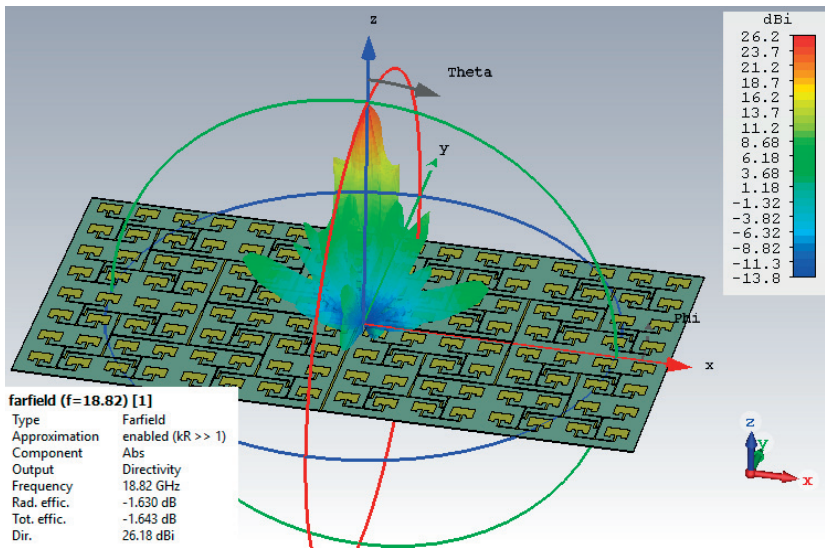

Figure 7.8: Far field directivity 3-D plot with total efficiency of around 70% (-1.63dB)

Chapter 8

Re-designing the TX Microstrip Patch Array for better Power Efficiency

The main disadvantage with the configuration in Section 6 however was in the angular beam width as we can see in the 3-D plots for the RX array design that the angular beam width with an 8x16 configuration was around 11°, whereas with a 4x8 configuration we were not only wasting precious space but radiating with an angular beam width of more than 24°, which means when working as a radar antenna system the power radiated outside the RX array's beam width would be wasted by the transmitter and both the angular beam widths must be similar in order to improve efficiency. Apart from that massive improvements were achieved when the second attempt was made using an 8x8 configuration in terms of gain, bandwidth, return loss and VSWR. The total size of the TX array would then increase to 143.5 x 140.5 mm^2 from the initial 143.5 x 73.45 mm^2 which is still very much within the project restrictions regarding the overall size of the system and the radiation efficiency would drop from approximately 68% to 64% as a consequence. The graphical representation of the S1, 1 parameter (return loss), VSWR and the 2-D/3-D plots of the array gain are given in Figs. 8.1-8.7 along with the new array configuration:

It must be observed here that the directivity of the array does not exhibit exponential growth. In fact it can generalized with the following equation:

$$\textbf{Far field gain for a single patch} + 3 \times \log_2 N$$

Where N is the total number of radiating elements in the array. This gives an approximate achievable directivity of 24 dB for an 8x8 configuration whereas per usual the actual results are a little short of that mark due to mutual coupling that is generally the resultant of space waves, higher order waves, surface waves and leaky waves of which the surface waves are dominant in cases where inter element spacing is greater than 0.5λ. Gain for the simulated single patch operating at 9.41 GHz as shown earlier was 5.98 dB with FR-4 as the dielectric material.

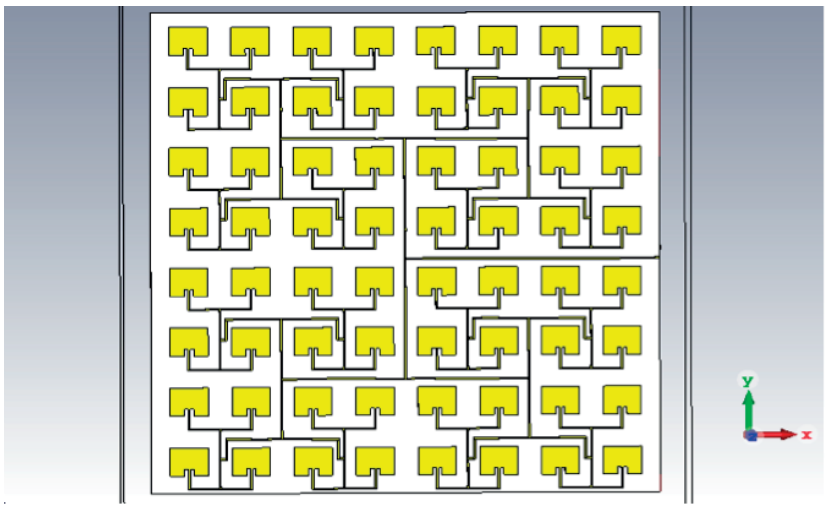

Figure 8.1: The new and final 8x8 array configuration with corporate feed using quarter wave transformers.

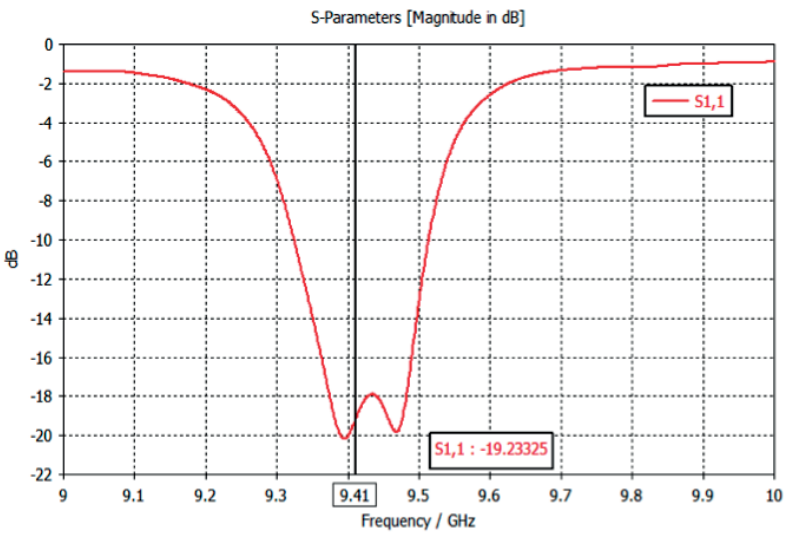

Figure 8.2: The S1, 1 parameter plot showing the array is resonant at 9.41 GHz.

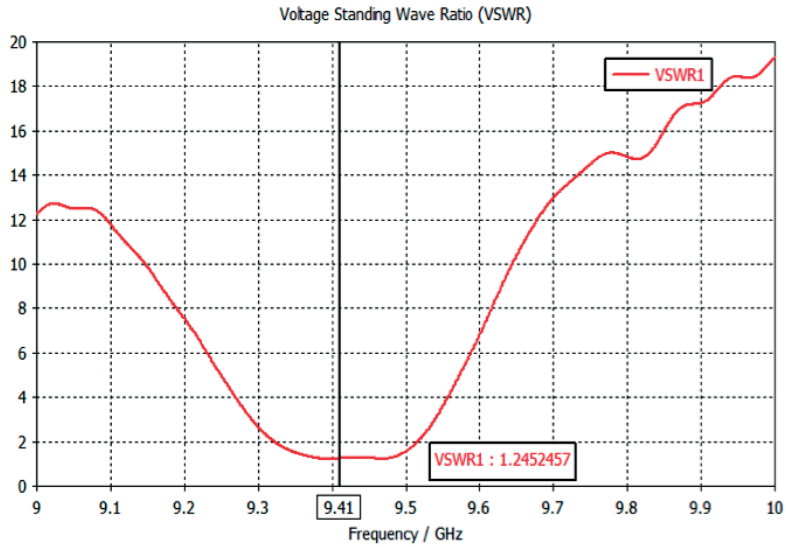

Figure 8.3: VSWR plot showing it to be less than 2 at around 1.24.

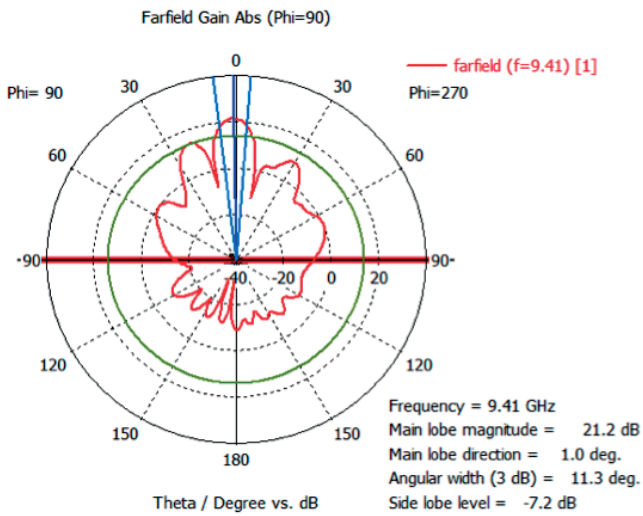

Figure 8.4: 2-D far-field gain plot with a main lobe magnitude of approximately 21 dB and an angular beam width of 11.3°.

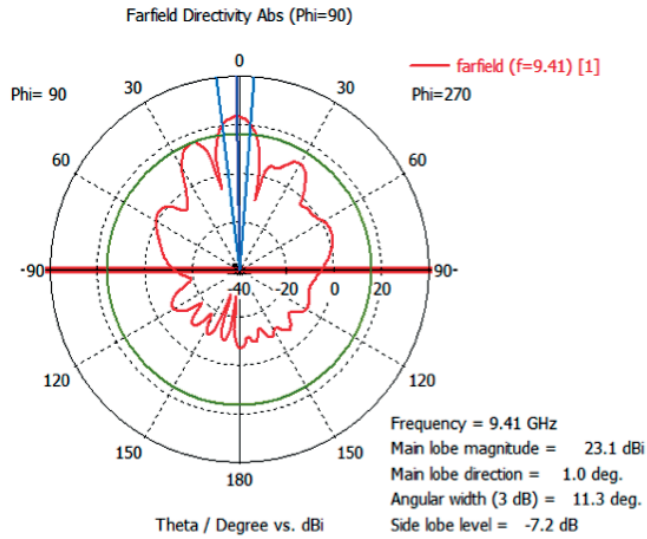

Figure 8.5: 2-D far-field directivity plot with a main lobe magnitude of approximately 23 dB and an angular beam width of 11.3°.

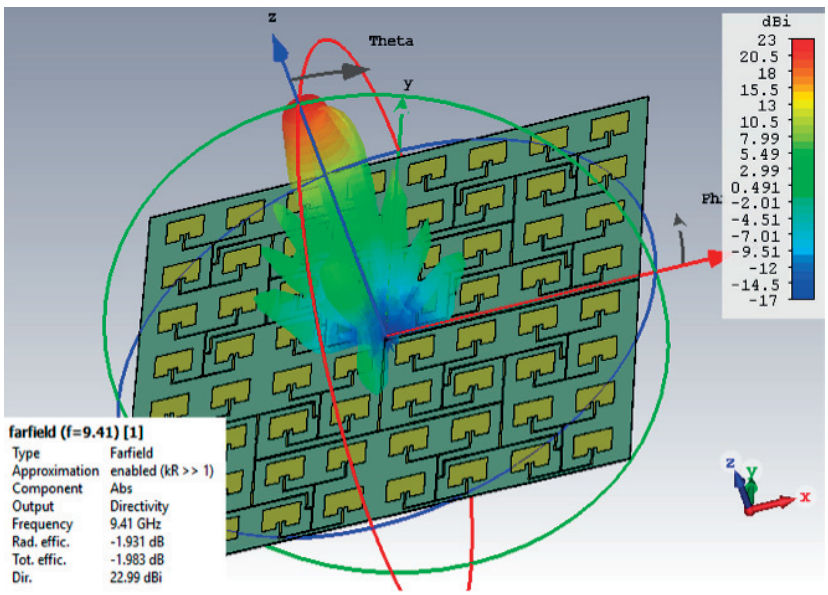

Figure 8.6: 3-D far-field directivity plot showing the radiation efficiency.

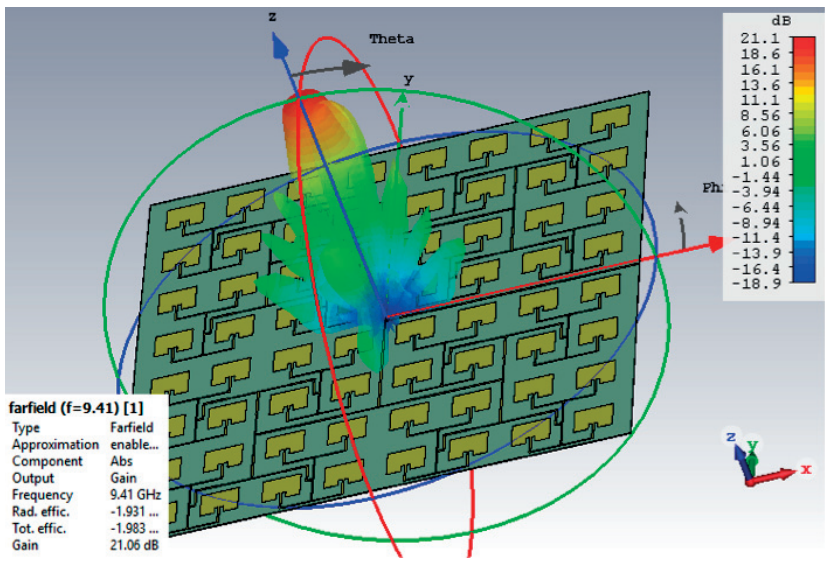

Figure 8.7: 3-D far-field gain plot showing the radiation efficiency.

Chapter 9

Designs for the Transponder

The most challenging part of the project was designing a suitable transponder i.e. the reflector antenna to be attached/mounted on the flying insect just because of the restrictions on its physical size and weight. Previous attempts made by other research groups had concluded that the thin wire dipole was the most reasonable design while some of them have even gone with a dual band miniature patch antenna. Most of the papers were incomplete in at least one sense of the requirements and to the best of authors' knowledge this is the single report which will comprehensively test all major designs for a harmonic transponder and then present a novel folded dipole foil antenna which will meet all the major requirements. The upper limit on the weight and dimensions of any transponder designed to be mounted on a flying insect in order to track it without impeding its flight trajectory should not be more than approximately 15 mm in length and 15 mg in weight. This begs the questions as to what should the choice be for the material and the diode used.

9.1 Thin Wire Transponder (Loop Dipole)

Firstly, we wanted to design the thin wire dipole antenna that is so widely used. For this purpose, we constructed a half wave dipole made out of copper with an inductive loop in the middle. The simple inductive loop provides a low resistance DC return path for any electrostatic charges that are generated during the rectifying action of the diode. It also protects the rather sensitive diodes from exposure to high electrostatic voltages which could cause damage. As we know, frequency conversion and multiplication processes cannot take place without the system having any harmonic sources and Schottky diodes being nonlinear elements have inherent capabilities to generate harmonics. The diode we used was from Sky Works Inc. with the model number SMS7630-079LF.

9.1.1 Design Parameters

The design parameters of a half wave dipole antenna based on the resonant frequency of 9.41 GHz are given below:

- Wavelength, $\lambda = c/f$
- Length of the half wave dipole antenna, L = 143 / f
- Feeding gap of the antenna, g = L / 200
- Radius of the wire, R = λ / 1000

The inductive loop was made out of fine copper wire with a diameter of approximately 2 mm (radius = 1mm) for operational purposes and the same radius as that of the antenna itself.

9.1.2 Simulations

These parameters were then calculated and the resulting numbers put into CST Studio Suite 2018 (Microwave/RF) to obtain the model shown in Fig. 9.1.

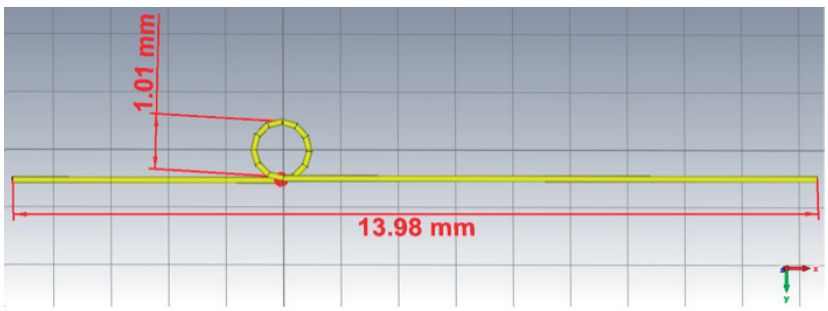

Figure 9.1: CST model for the half wave length loop-dipole antenna

The return loss results were not very promising with the fundamental frequency registering a return loss of approximately -11dB and the second harmonic registering a return loss of approximately -13 dB.

The gain for the designed half wave dipole antenna at both the fundamental and second harmonic frequency coincided well with the theoretical values, with the radiation pattern of the half wave dipole slightly narrower than that of the Hertzian dipole. The 2-D and 3-D plots with a cut angle θ =0° are shown below in Figs. 9.3, 9.4, 9.5 and 9.6..

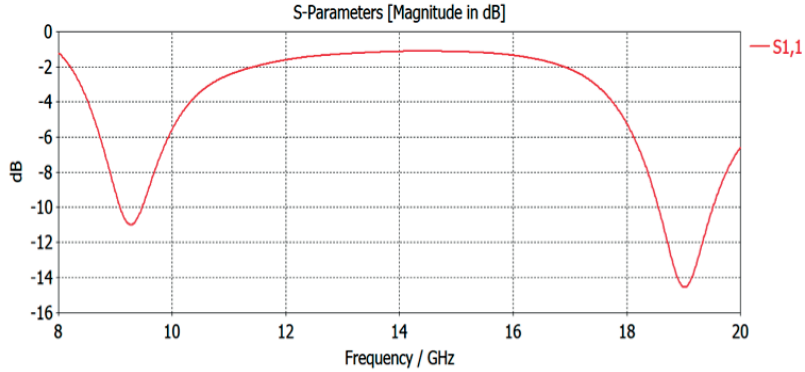

Figure 9.2: S1,1 parameter results for the thin wire half wave length loop-dipole antenna

9.2 Microstrip Patch Transponder

The next design that we tried was a dual band microstrip patch antenna. For this purpose, we decided to experiment with the same materials as we used in the RX array design. The substrate chosen was FR-4, with a thickness of 0.254 mm and the simple patch designs for fundamental frequencies of 9.41 GHz and 18.82 GHz from Chapters 4 and 7 were connected together with a discrete port in CST Studio Suite 2018 (Microwave/RF) to mimic the Schottky diode chosen which had a resistance of max resistance of 8Ω. The design is shown in Fig. 9.7.:

9.2.1 Fringing Fields

According to the fore mentioned micro strip patch antenna theory, it was expected that the patch antenna would have a much higher gain due to the presence of a substrate and the inherent property of a patch to radiate most of the power normal to its surface. Because the radiation pattern of a micro strip patch antenna is unidirectional broadside to the patch, all rectangular patch antennas will have a main lobe (beam peak) in the z-direction. The pattern expressions for the rectangular patch can be easily approximated by applying antenna theory, especially using the transmission line model viewpoint of two radiating slots. This assumes the region between the patch and the ground plane acting as a half wavelength transmission line that is open circuited at one end. The electric field lines associated with the standing wave mode inside the patch can be seen in Fig. 4.4. The fringing fields shown at the ends are exposed to the upper half space (z>0) and these fields, unlike any other antenna, are responsible for the radiation. The fringing fields at the left and right halves of the patch are opposite in sign, meaning they are 180° out of phase and equal in magnitude. These same electric fields when viewed from the top, shown in Fig. 9.8, are back in phase as a consequence of the half wavelength separation which leads to a reinforcement of radiation broadside to the patch.

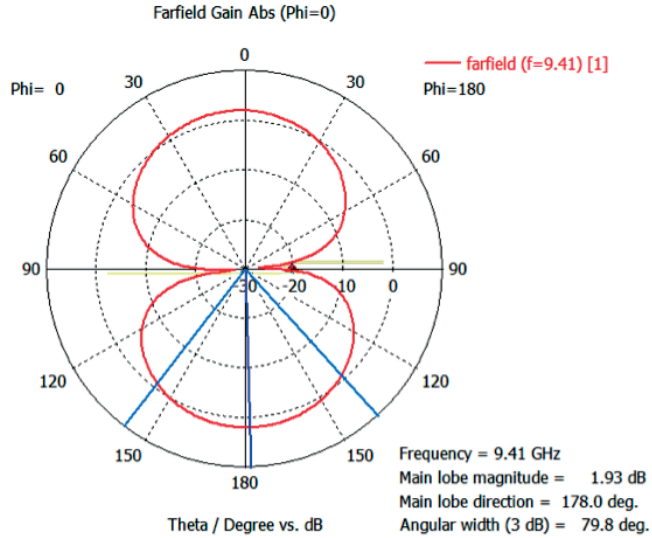

Figure 9.3: Polar plot of Far field Gain of approximately 2dB achieved at 9.41 GHz for the thin wire loop dipole transponder with 80° angular beam width & ϕ=0°

The principle plane patterns are given as:

$$F_E = cos(\frac{\beta L}{2} sin\theta); \qquad E - plane, \Phi = 0^\circ$$

$$F_H = \cos\theta \left(\frac{\sin\left(\frac{\beta\Omega}{2}\sin\theta\right)}{\left(\frac{\beta\Omega}{2}\sin\theta\right)} \right); \qquad H - plane, \Phi = 90^\circ$$

9.2.2 Simulations

The simulated radiation patterns confirm this discussion and are presented in 2-D and 3-D forms in Figs. 9.9-9.16.:

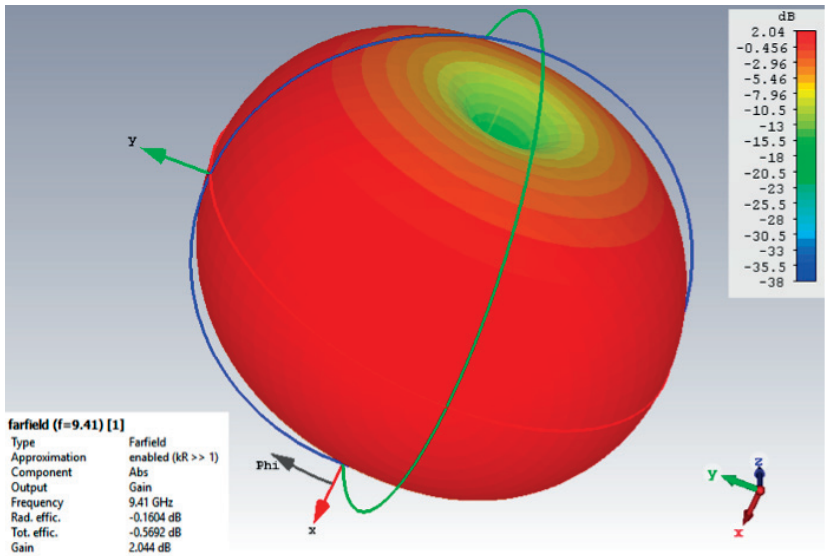

Figure 9.4: Far field gain 3-D plot for the thin wire loop dipole transponder showing total efficiency of approximately 88% (-0.5692 dB)

9.2.3 Power Efficiency

The power radiated vs power accepted graph is especially important because it is indicator of what the efficiency of the proposed transponder is, as we can see the power outgoing and power in going into all ports. This is of course taking into account the unavoidable metal losses in copper. A patch antenna, although being much better in terms of its performance for this particular application compared to the thin wire half wavelength loop dipole will always have excess harmonic radiations on a downside and this can be seen in the graph above where power is lost at unwanted frequency levels. The transponder is radiating outwards approximately 0.43 W of the 0.5 W it is getting (accepting) at the fundamental frequency and at the second harmonic, it is radiating outwards approximately 0.45 W of the 0.5 W it is getting (accepting). This accounts for a total power efficiency of 85 % and 91 % at the fundamental and second harmonic frequencies respectively. A measure of the impedance matching of loads to the characteristic impedance of the transmission line which in this case is a Schottky diode can be seen from the graphical representation of the voltage standing wave ratio in Fig. 9.17.:

Although the results of the miniature micro strip patch antenna were the most promising out of all the transponder designs that we tried, there was one hidden disadvantage though, which was only realized after manufacturing and it was regarding the weight. The patch transponder weighed in at over 100mg which was practically useless in such an intricate application.

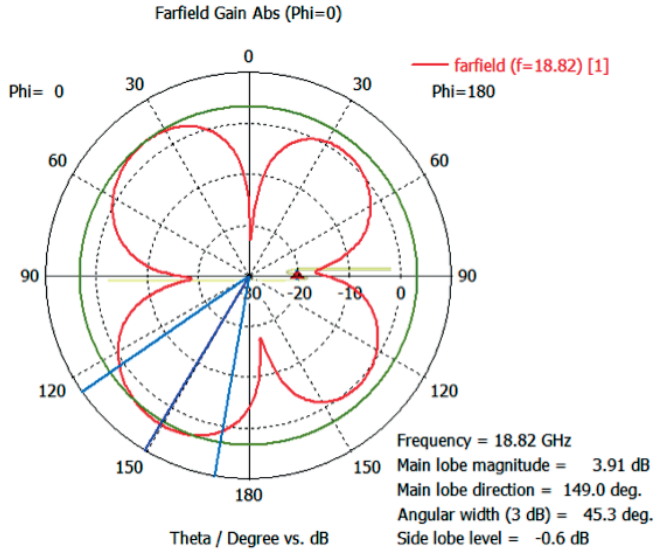

Figure 9.5: Polar plot of Far field Gain of approximately 4dB achieved at 18.82 GHz for the thin wire loop dipole transponder with 46° angular beam width & ϕ=0°

9.3 Folded Dipole Transponder

9.3.1 Introduction

After these two designs, we were forced to think out of the box and after some discussion we realized that none of the previous attempts at building transponders for harmonic radars had thought of combining two dipoles i.e. a folded dipole and construct it out of an extremely thin copper foil, so we decided to follow this design path. A folded dipole is just a simple dipole antenna but with its arms folded back around and connected to each other, which as a result makes a loop as shown in Fig. 9.18.:

The gap in between, denoted by d here is usually very small compared to the total length L of the antenna. In short, d $\ll$ L and d $\ll \lambda$. The folded dipole is famous for various reasons including:

- Impedance Matching (easy to match)
- Simple and easy to manufacture design
- Rigid Structure
- Wide bandwidth compared to half wave length dipole

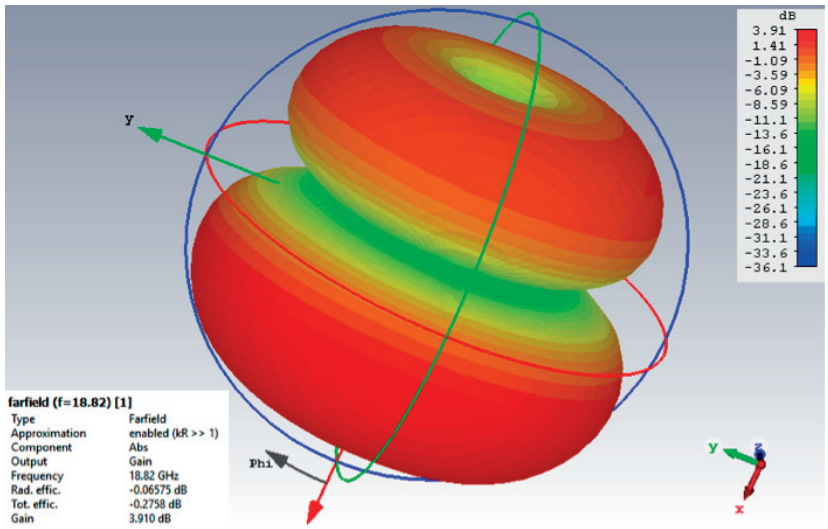

Figure 9.6: Far field gain 3-D plot for the thin wire loop dipole transponder showing total efficiency of approximately 94% (-0.2758 dB)

9.3.2 Analysis – Mode of Operations and Radiation Resistance

The method to analyze a folded dipole is rather simple because we can decompose the current flow through a folded dipole into two modes, namely, the transmission mode currents and antenna mode currents and then superimposing them to obtain a complete model as shown in Fig. 9.19:

Due to the fact that there are two closely spaced and equal currents travelling in opposite directions, they cancel each other out in the far field in the transmission line mode meaning a virtual short circuit occurs at the points labelled as x in the figure above, which, for a single voltage source yields the circuit model given in Fig. 9.20.:

The impedance seen by the source then becomes the following according to transmission line theory: [17]

$$Z_t = \jmath Z_o \tan \beta \frac{L}{2}$$

And therefore,

$$I_t = \frac{V}{2} \frac{1}{Z_t} \tag{9.1}$$

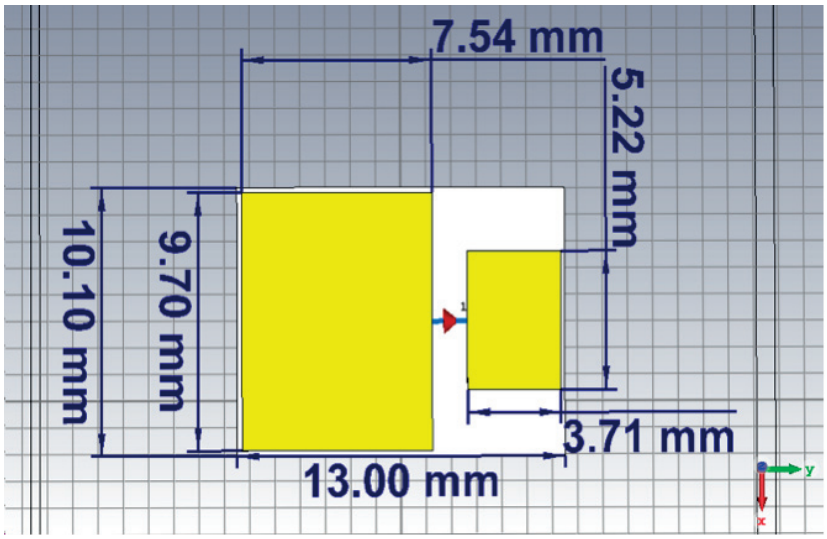

Figure 9.7: CST model for the Dual frequency Microstrip Patch Transponder Antenna

For the antenna mode, the points c and d can be connected together as they are at the same potential, as well as the two line currents. The points marked as o can then be treated as locations of open circuits because of no cross over between the two halves of the folded dipole. We can make this assumption more clear by seeing Fig. 9.21 where we now have a dipole with current I_a , powered by a V / 2 voltage source:
But, for a dipole, we know how to calculate impedance Z d and I a then becomes.

$$I_a = \frac{V}{2}\frac{1}{Z_d} \tag{9.2}$$

The voltage source feeding the folded dipole will then have a total current of

$$I_f = I_t + \frac{I_a}{2} \tag{9.3}$$

Which will give the input impedance of the folded dipole to be

$$Z_f = \frac{V}{(I_t + I_a/2} \tag{9.4}$$

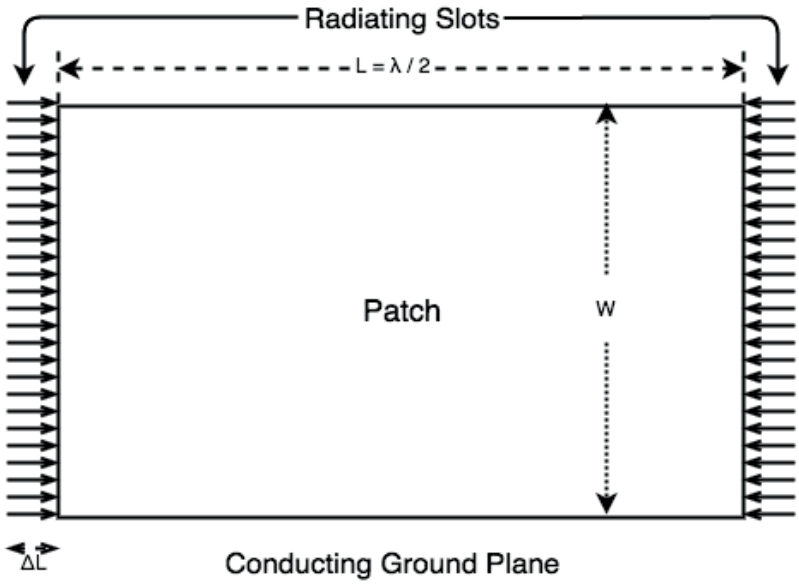

Figure 9.8: Top view of the reinforcing electric field lines in a Microstrip Patch [10]

$$Z_f = \frac{4Z_t Z_d}{2Z_d + Z_t} \tag{9.5}$$

Hence, for full wave folded dipole this would mean an input impedance of 4 Z_d i.e. 775.6 Ω , as $Z_t = \infty$ and $Z_d = 193.9$ Ω for a full wave length dipole.

The radiation characteristics of a folded dipole are exactly the same as a standard half wave length dipole as both arms of the antenna carry identical, half wave sinusoidal current distributions. The directivity of the folded dipole is the same as that of the half wave length dipole because the currents in both wires are so close to each other that we treat them as a single half wave length of wire.

9.3.3 Simulations

The constructed folded dipole in CST Studio Suite 2018 (Microwave/RF) is shown in Fig. 9.22.:

The cylinder placed at the bottom of the folded dipole mimics the body of the Bogong Moth. The approximate body length of this species is approximately 35 mm and the thin foil folded dipole is around 30 mm. The cylinder was placed at a distance of 2 mm from the antenna itself and it was filled up with half water

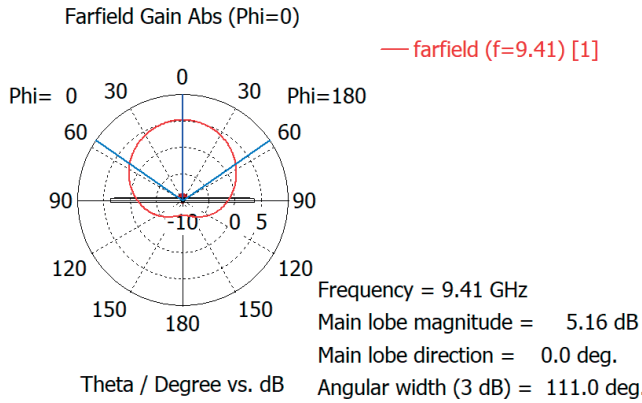

Figure 9.9: Polar plot of Far field Gain of approximately 5.2dB achieved at 9.41 GHz for the microstrip patch transponder with 111° angular beam width & ϕ=0°

and half sand which to best of authors' knowledge must be the constituents of the targets body. This had a dielectric constant of approximately 14 which provided a great challenge in maintain the gain to be positive as the dielectric i.e. the cylinder mimicking the insect's body was relatively quite thick in terms of microwave theory. The width on the upper arm of the folded dipole shown above was adjusted to be around 0.32 mm whereas the lower arm had a width of about 0.08 mm. The thickness of the antenna was kept at 0.005 mm. The feeding method used was the discrete port option where the resistance of the port was kept at 8 Ω to simulate the Schottky Diode chosen mentioned earlier. The S11 and VSWR results were promising after minor tweaks in the design parameters and are shown in Figs. 9.23 and 9.24.:

9.3.4 Effects on the Efficiency

The power efficiency was expected to drop compared to the microstrip patch antenna design but the performance was still acceptable and the total efficiency of the system was about 32 %, shown in Fig. 9.25.:

It was found that wider antenna arms in a folded dipole increase gain but that meant a decrease in the thickness, hence moving towards a foil antenna design from the initial simple thin wire half wavelength folded dipole. The presence of

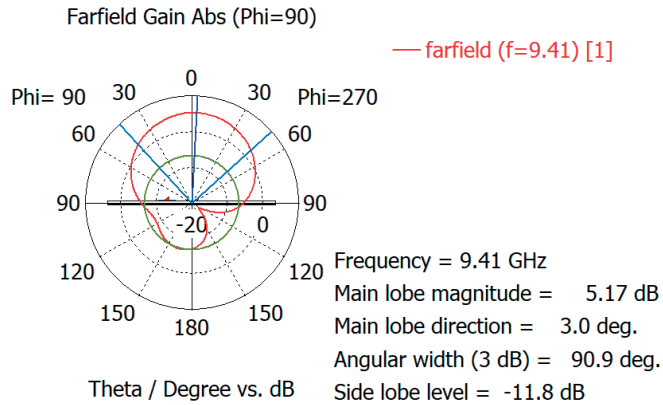

Figure 9.10: Polar plot of Far field Gain of approximately 5.2dB achieved at 9.41 GHz for the microstrip patch transponder with 91° angular beam width & ϕ=90°

the cylinder i.e. the moth's body also affected the gain immensely. The simulated results are shown in Figs. 9.26-9.29.:

9.3.5 Performance Optimization

The thinnest possible cut of commercially available copper/silver/gold foil is 0.5 μm (0.0005 mm) so we decided to go as close as possible to that limit. The aim here is to keep a fix volume (0.016 cubic mm) for the wider folded dipole arm (usually the one with the feed/diode) and reduce the thickness of the copper foil while, at the same time, increasing the width. The results were profound when the width of the feed arm of the folded dipole was increased to 0.64 mm and the thickness of the foil was decreased to 0.0025 mm as the gain of the antenna increased by approximately 1 dB and the efficiency of the transponder system was now at approximately 37 %, a 5 % increase compared to the previous parameters used.

Such small alterations are often made to thin folded dipole antennas to compensate for the fact that the propagation velocities in the common mode and TEM mode are different because the balance between electrical energy storage outside and inside the dielectric which supports the two arms is different in each mode. The final iteration for the folded dipole design was made with the two parameters for the dipole arms kept at 0.64 mm and 0.08 mm for the lower (feed) and upper arms respectively. The design is shown in Fig. 9.30 with the measurements along with the graphical results of the S 1,1 parameter, VSWR, power radiated and the

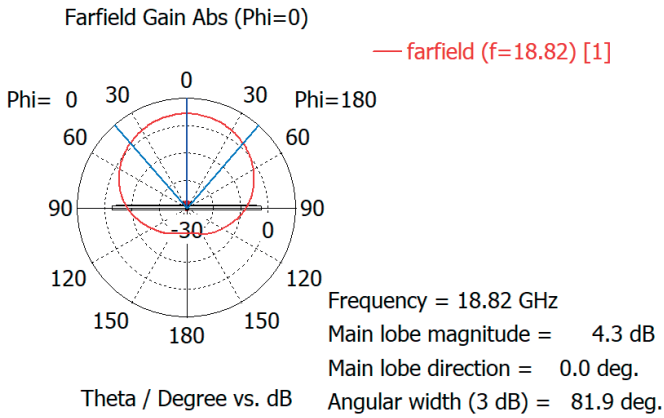

Figure 9.11: Polar plot of Far field Gain of approximately 4.3dB achieved at 18.82 GHz for the microstrip patch transponder with 82° angular beam width & ϕ=0°

gain of the antenna in Figs. 9.31-9.37.:

The distance between the wet sandy soil cylinder acting as the moth's body and the transponder itself is kept at 2 mm. The far field results from the CST simulations show that the directivity of the antenna at the fundamental frequency 9.41 GHz is approximately 6.5 dB while it is approximately 7.75 dB at the second harmonic 18.82 GHz. The power stimulated by the discrete port in all cases was 0.5 W by default. The -3dB bandwidth for the folded dipole transponder at the fundamental frequency is 110 MHz. At the second harmonic, the system had a -3dB bandwidth of 210 MHz. Similarly, the -10 dB bandwidth at the fundamental frequency is 35 MHz and at the second harmonic, the system has around 50 MHz. All bandwidth measurements are approximate and are calculated after placing the cylinder containing water and soil which negatively affects these measurements.

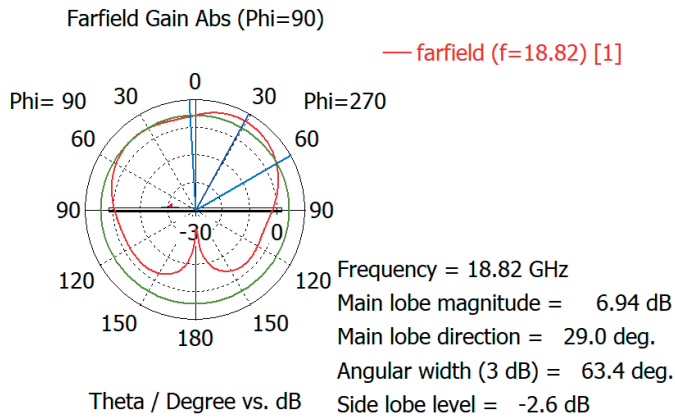

Figure 9.12: Polar plot of Far field Gain of approximately 7dB achieved at 18.82 GHz for the microstrip patch transponder with 64° angular beam width & ϕ=90°

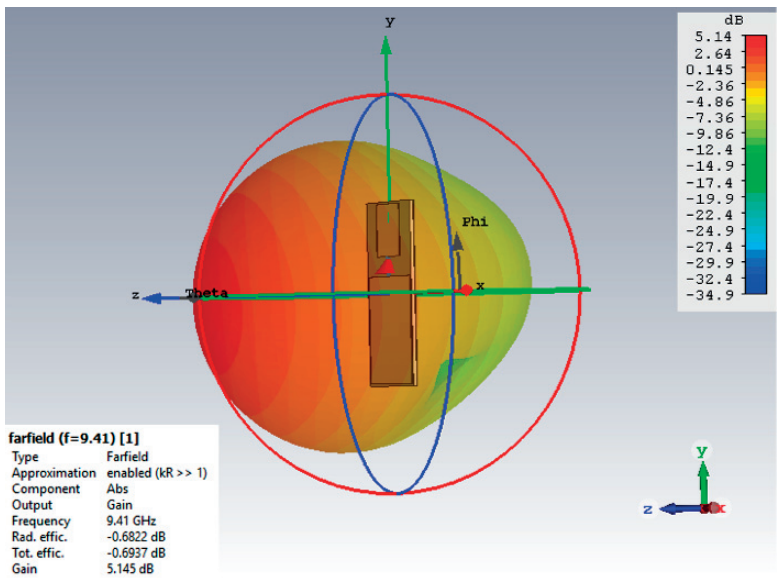

Figure 9.13: Far field gain 3-D plot for the microstrip patch transponder at 9.41 GHz showing total efficiency of approximately 86% (-0.6937 dB)

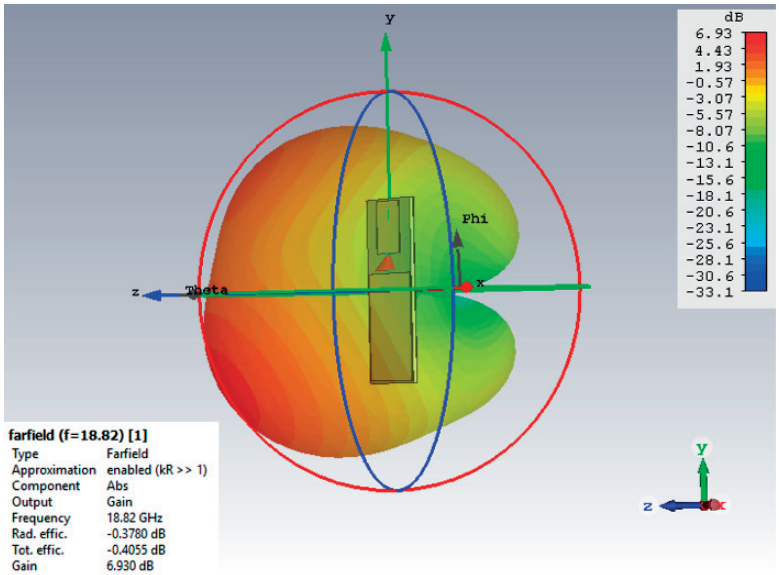

Figure 9.14: Far field gain 3-D plot for the microstrip patch transponder at 18.82 GHz showing total efficiency of approximately 91% (-0.4055 dB)

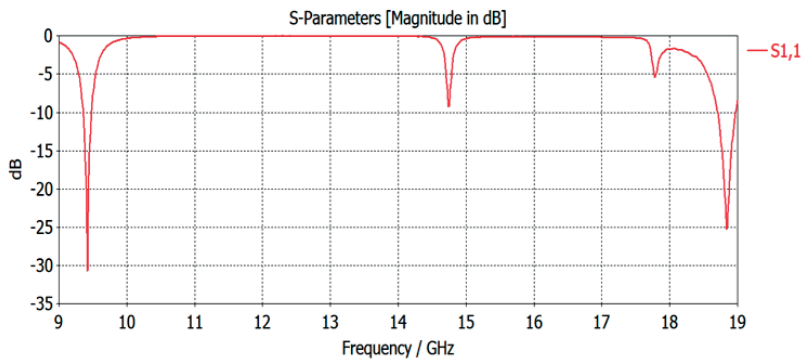

Figure 9.15: S1,1 parameter results for the microstrip patch transponder showing a return loss of more than -30dB at the fundamental frequency and around -25dB at the second harmonic

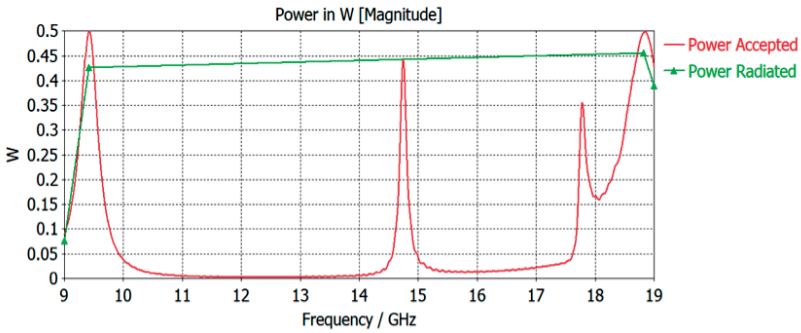

Figure 9.16: Power Efficiency results for the microstrip patch transponder showing power accepted vs power radiated

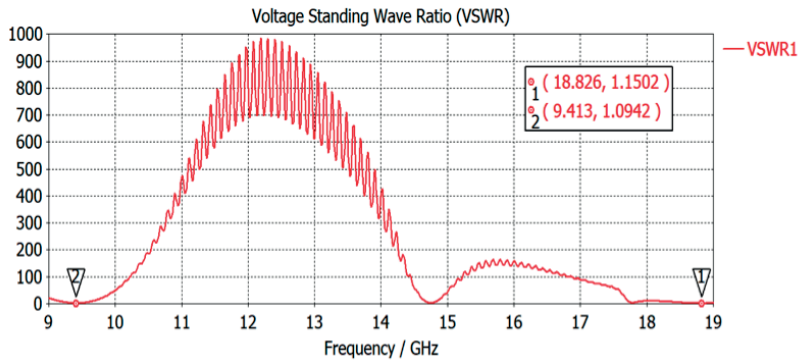

Figure 9.17: Voltage Standing Wave Ratio results for the microstrip patch transponder

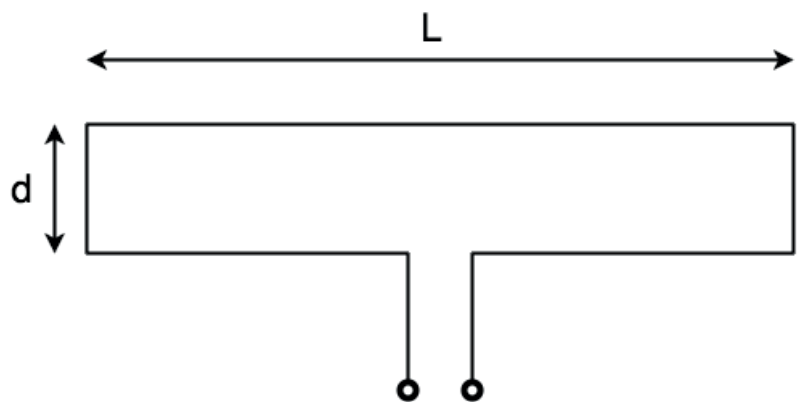

Figure 9.18: Basic Structure and Parameters of a Folded Dipole Antenna [17]

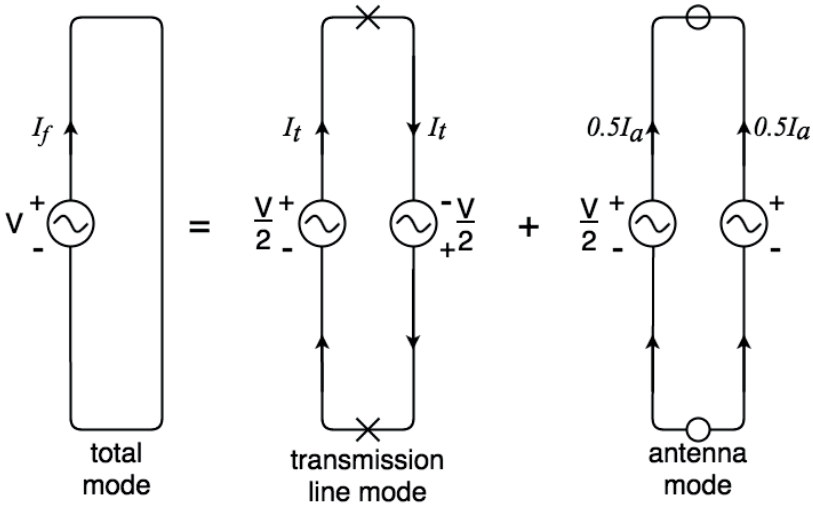

Figure 9.19: Transmission Modes of a Folded Dipole Antenna [17]

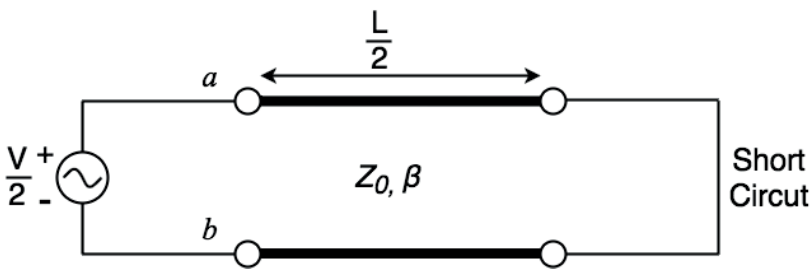

Figure 9.20: Virtual Short Circuits at the points labeled as X in Fig. 9.19. [17]

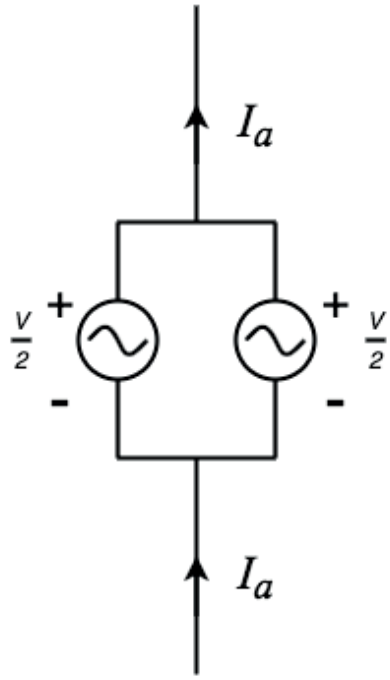

Figure 9.21: Virtual Open Circuits at the points labeled as O in Fig. 11.19. [17]

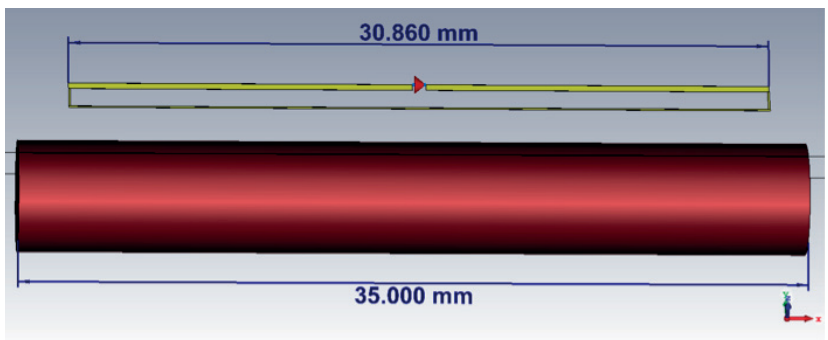

Figure 9.22: CST model for the proposed folded dipole transponder with a wet sandy soil cylinder depicting the body of the Bogong moth

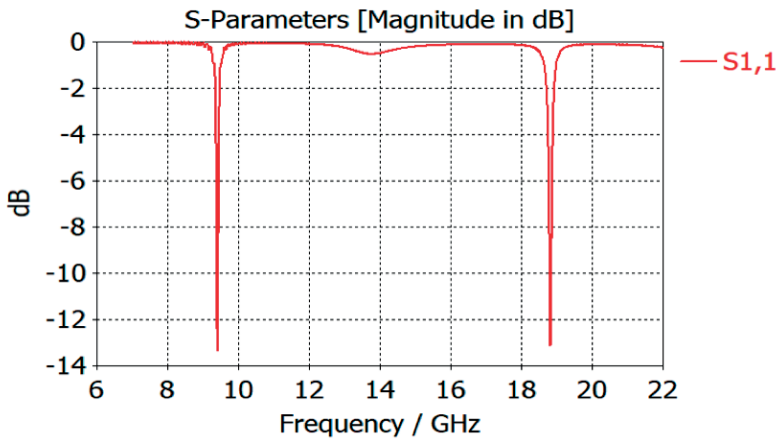

Figure 9.23: S1,1 parameter results for the initial folded dipole transponder showing a reflection coefficient of approximately -14dB at both the fundamental and second harmonic frequencies

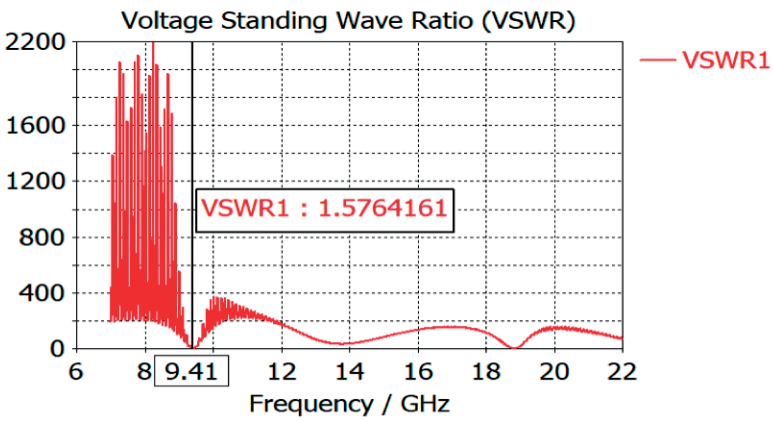

Figure 9.24: Voltage Standing Wave Ratio results for the initial folded dipole transponder

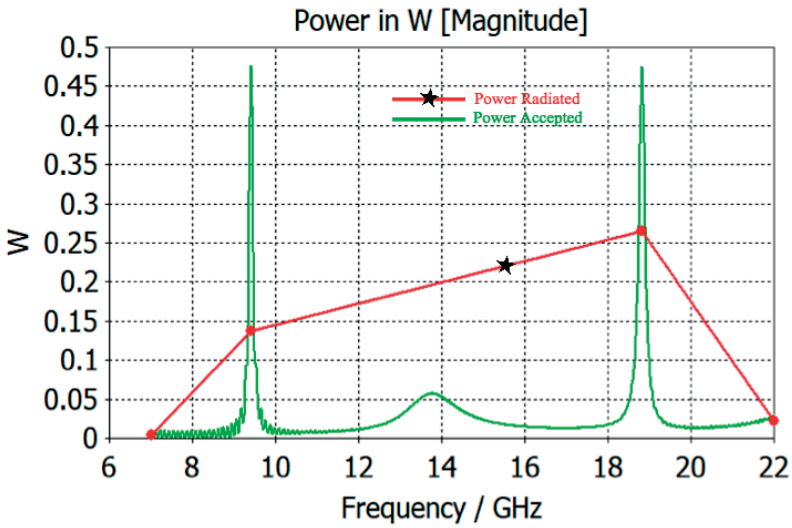

Figure 9.25: Power Efficiency results for the folded dipole transponder showing power accepted VS power radiated

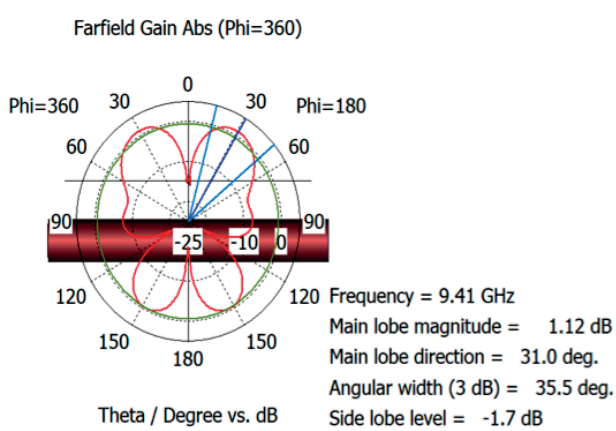

Figure 9.26: Polar plot of Far field Gain of approximately 1.2dB achieved at 9.41 GHz for the folded dipole transponder with 36° angular beam width & ϕ=360°

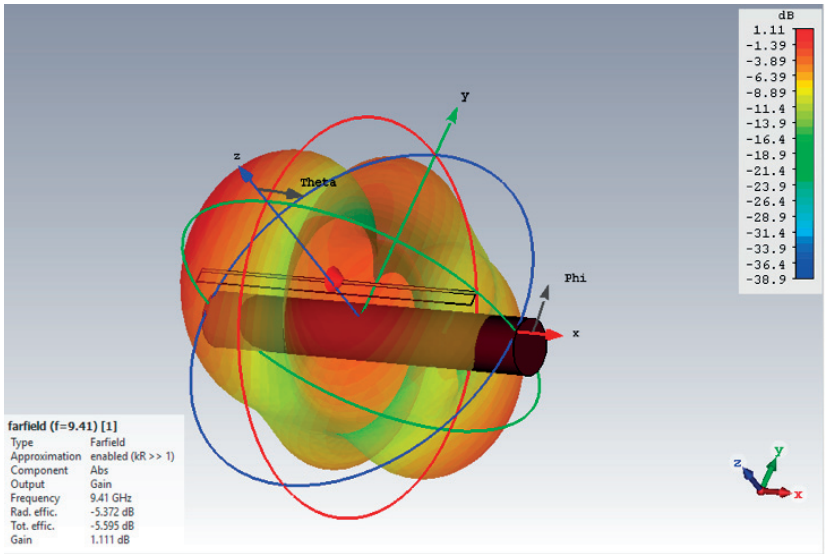

Figure 9.27: Far field gain 3-D plot for the folded dipole transponder at 9.41 GHz showing total efficiency of approximately 32% (-5.372 dB)

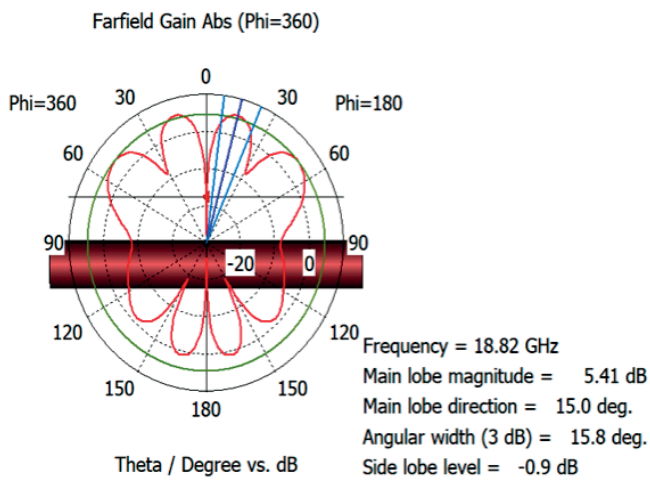

Figure 9.28: Polar plot of Far field Gain of approximately 5.41dB achieved at 18.82 GHz for the folded dipole transponder with 16° angular beam width & ϕ=360°

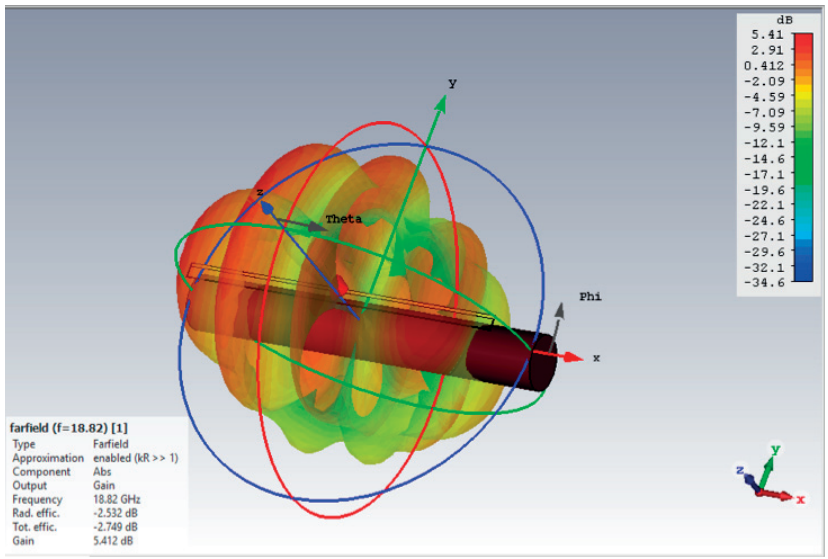

Figure 9.29: Far field gain 3-D plot for the folded dipole transponder at 18.82 GHz showing total efficiency of approximately 53% (-2.749 dB)

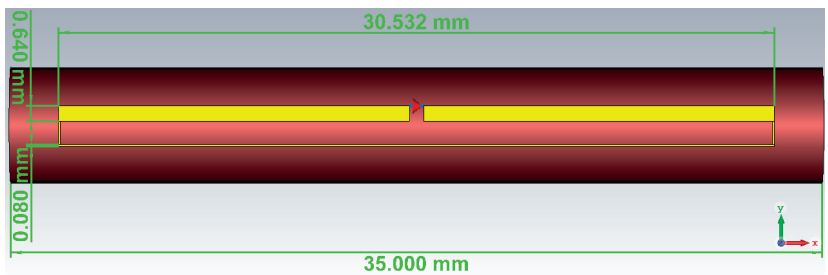

Figure 9.30: CST model for the improved Thin Foil Folded Dipole Transponder

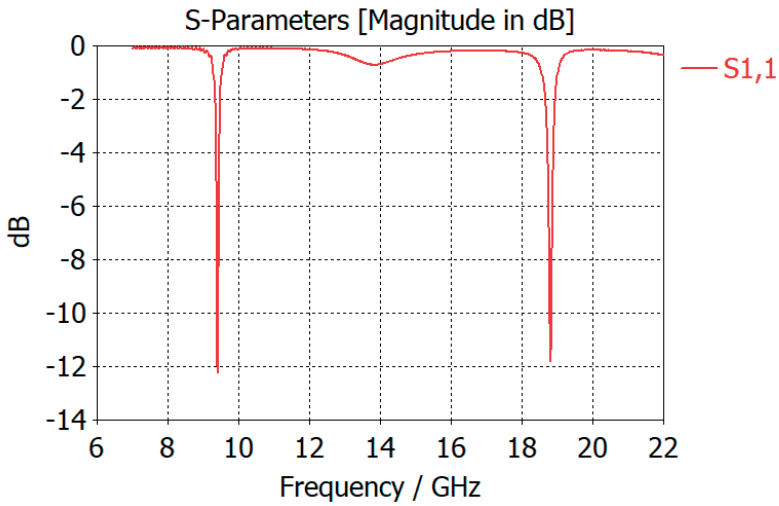

Figure 9.31: S1,1 parameter results for the improved thin foil folded dipole transponder showing a reflection coefficient of approximately -12dB at both the fundamental and second harmonic frequencies

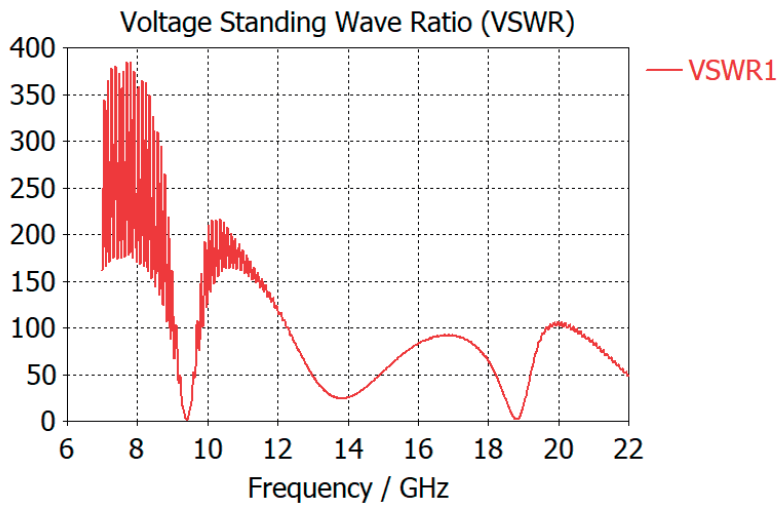

Figure 9.32: Voltage Standing Wave Ratio results for the improved thin foil folded dipole transponder

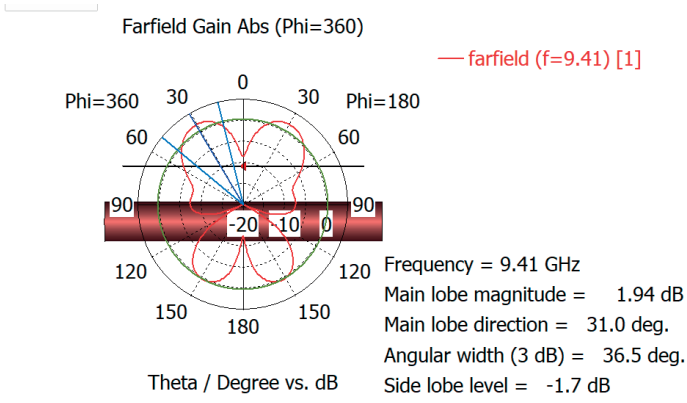

Figure 9.33: Polar plot of Far field Gain of approximately 2dB achieved at 9.41 GHz for the improved thin foil folded dipole transponder with 37° angular beam width & ϕ=360°

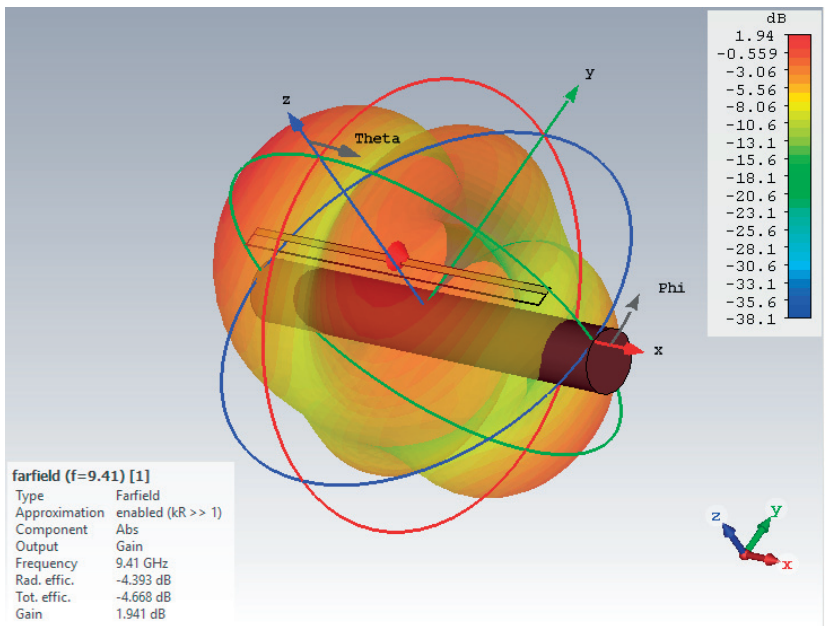

Figure 9.34: Far field gain 3-D plot for the improved thin foil folded dipole transponder at 9.41 GHz showing total efficiency of approximately 38% (-4.393 dB)

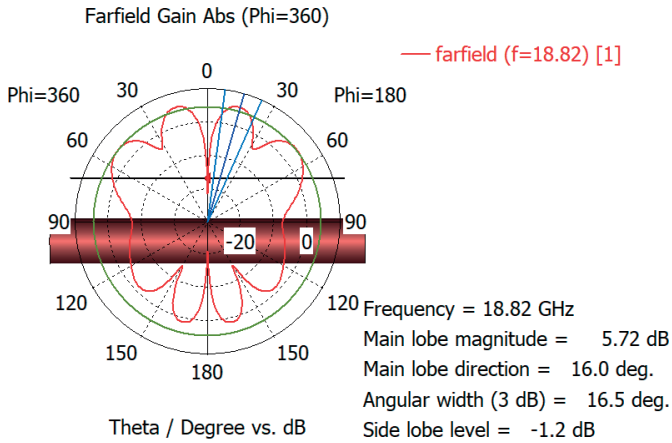

Figure 9.35: Polar plot of Far field Gain of approximately 5.8dB achieved at 18.82 GHz for the improved thin foil folded dipole transponder with 17° angular beam width & ϕ=360°

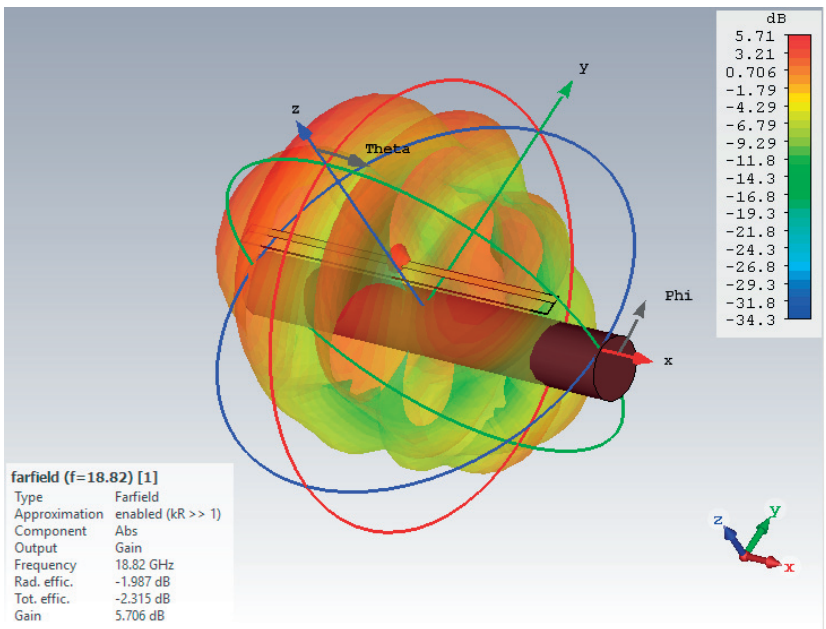

Figure 9.36: Far field gain 3-D plot for the improved thin foil folded dipole transponder at 18.82 GHz showing total efficiency of approximately 64% (-1.987 dB)

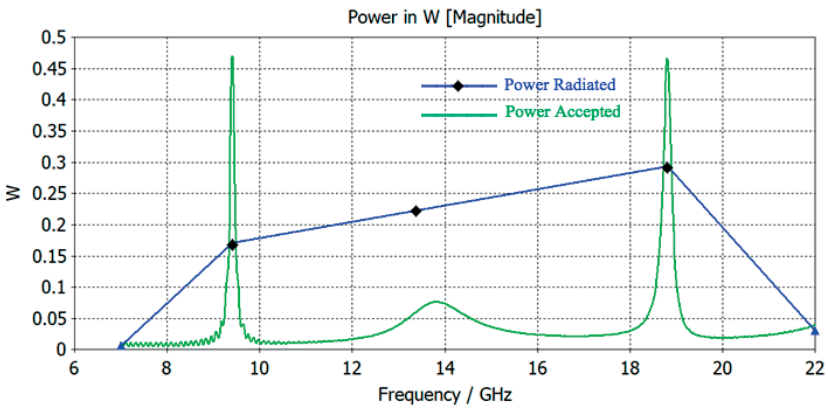

Figure 9.37: Power Efficiency results for the improved thin foil folded dipole transponder showing power accepted VS power radiated

Chapter 10

Propagation Model, Measurements & Results

10.1 The Link Budget

A link budget accounts for all the losses and gains from the transmitter, the medium, to the receiver, hence the word "budget". We begin with the output power capacity of the transmitter and sum the system gains and losses to determine the level of power that is actually delivered to the receiver. The power available at the receiver should always be in excess of what is required for a minimum level of performance in order to have a reliable link.

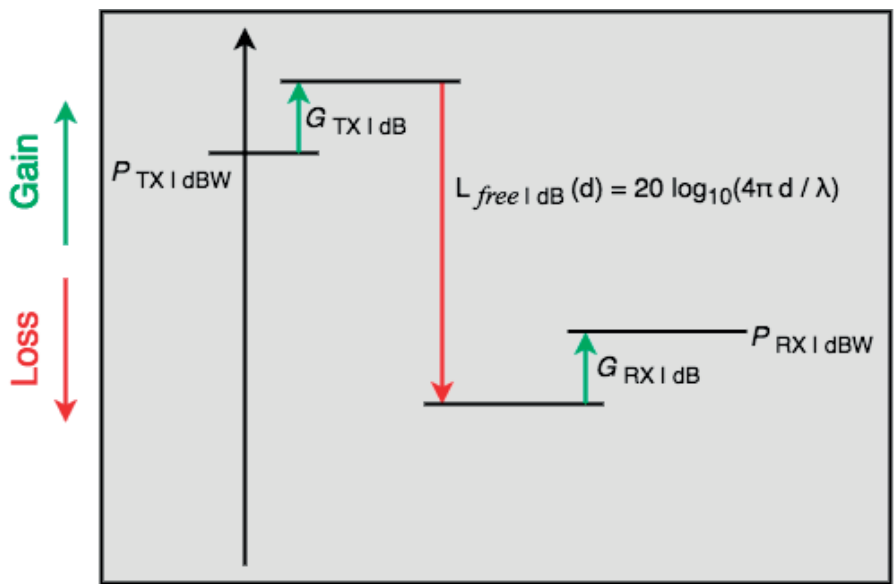

Figure 10.1: The Link Budget in the normal case [19]

Here, P_{TX} is the transmitted power in dBm, G_{TX} is the antenna gain at the transmitter, L_{FREE} is the propagation losses in dB between the transmit and

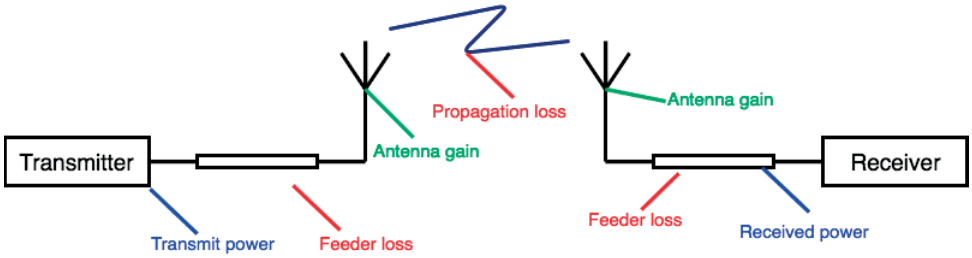

Figure 10.2: The normal case model

receive antennas, G_RX is the antenna gain at the receiver and P_{RX} is the received power in dBm. To provide a margin of safety for a reliable link as mentioned earlier, the level of received power in excess of that required is referred to as the fading margin. It is most often tied to the receiver's sensitivity. This sensitivity, if simply put, specifies the minimum RF input power required to produce a usable output signal.

One must take impedance mismatch loss into account also and the most common indicator for this purpose is the VSWR and is typically specified as some maximum value over the operational bandwidth, e.g. VSWR $<$ 2:1. Equation 10.2 is used to convert the VSWR of the system to mismatch loss in dB.

Putting Frii's law into the link budget we get figure 10.1 The received power decreases as $1/d^2$ which means a propagation exponent of n=2.

Free-space loss calculations are only valid in the far-field of the antenna i.e. far beyond the Rayleigh distance which is given in equation 10.4.

$$P_{dBm} = 10\log(P_{Watts}) + 30 \tag{10.1}$$

$$ML = -10\log\left\{1 - \left[\frac{VSWR - 1}{VSWR + 1}\right]^2\right\} \tag{10.2}$$

$$dBi = dBd + 2.15 \tag{10.3}$$

$$d_R = 2\frac{L_a^2}{\lambda} \tag{10.4}$$

As an electro magnetic wave propagates through free space, the power density per unit area decreases in propagation to the frequency and the square of the distance traveled. This phenomenon gives rise to the classical free space loss equation given in equation 10.5.

$$L_{FREE|dB} = 32.45 + 20log(d) + 20log(f) \tag{10.5}$$

While free space path loss is often used in link budget calculations, it must be noted that such an environment is not realistic in earth based telemetry links and for many scenarios, the use of such a propagation model does not result in a realistic link budget. Equation 10.6 gives the received power with antenna gains G_{TX} and G_{RX}.

$$P_{RX|dBW}(d) = P_{TX|dBW} + G_{TX|dB} - L_{FREE|dB}(d) + G_{RX|dB} \tag{10.6}$$

In the case of our transponder design, since there are two different frequencies involved, there had to be a conversion loss. One method of describing the transponder from a system point of view is through its cross sectional area. If A_H is the harmonic cross sectional area of the transponder, P_H is the power transmitted by the transponder at the harmonic, G_H is the gain of the transponder at the harmonic and P_F is the power incident upon the transponder at the fundamental frequency in watts per square meter, then the harmonic cross sectional area can be given by equation 10.7.

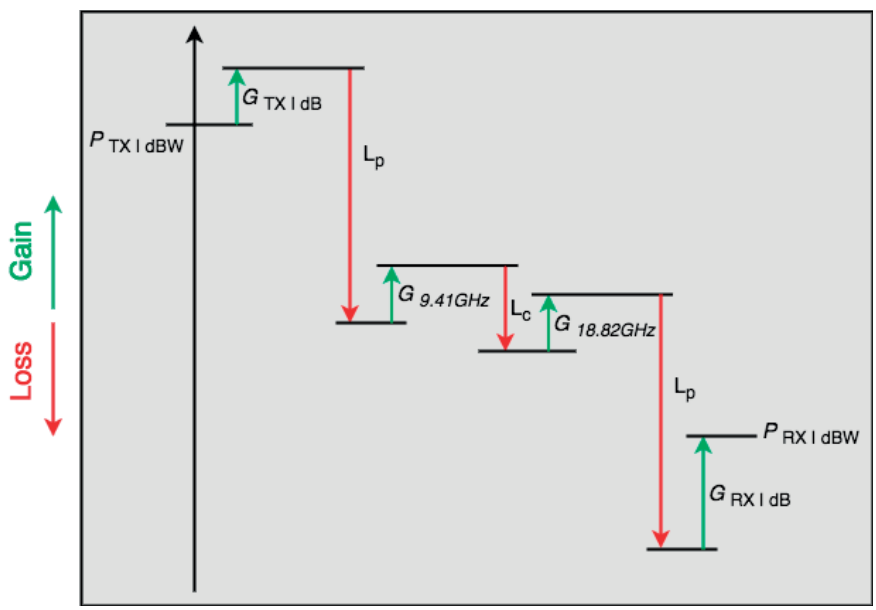

Figure 10.3: The Link Budget in our system

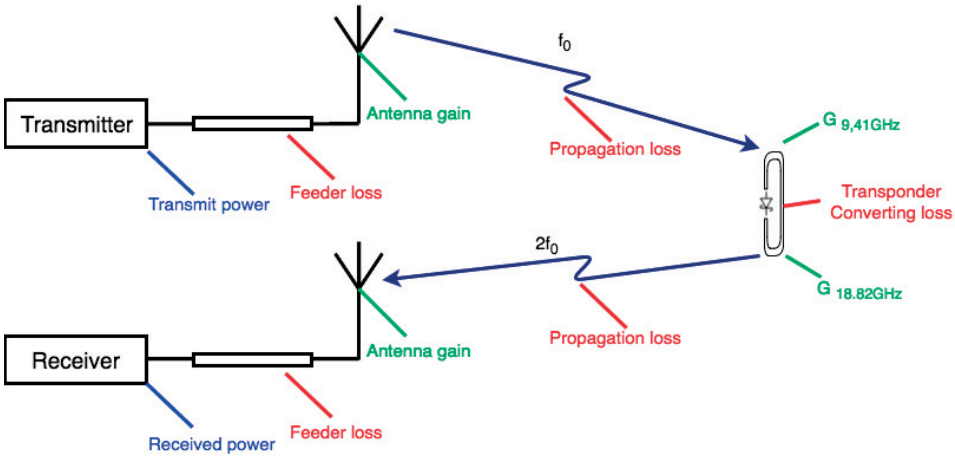

Figure 10.4: The model of our system

$$A_H = \frac{P_H G_H}{P_F} \tag{10.7}$$

Power incident on the transponder at the fundamental frequency can then be given by replacing radar cross section by the harmonic cross section in the radar range equation, shown in equation 10.8.

$$P_F = \frac{P_R G_{TX}}{4\pi r^2} \tag{10.8}$$

Here, P_R is the radar transmit power at fundamental frequency. It must be noted that in this case, the effective isotropic radiated power i.e. EIRP becomes the power transmitted by the transponder at the harmonic multiplied by the gain of the transponder antenna at the harmonic, given in equation 10.9.

$$P_H G_H = A_H \frac{P_R G_{TX}}{4\pi r^2} \tag{10.9}$$

The link from the transponder back to the radar then by the Frii's formula is given by equation 10.10 i.e. the power received at the second harmonic by the radar; P_{RX}.

$$P_{RX} = P_H \frac{G_H G_{RX} \lambda_H^2}{4\pi r^2} \tag{10.10}$$

Theoretically then, the ratio between P_{OUT}, which is the power received by the radar at the harmonic and P_{IN}, which is the power transmitted by the radar at the fundamental frequency is given by equation 10.11.

$$\frac{P_{OUT}}{P_{IN}} = \frac{A_H G_{TX} G_{RX}}{4\pi} \frac{\lambda_H^2}{4\pi r^4} \tag{10.11}$$

Since, analyzing the conversion efficiency of such an electrically small transponder proved to be difficult and quite complex in CST Studio Suite, we opted to analyze the frequency response instead.

In the most simplest form, if a sine wave is generated in a system at a given frequency, then an equivalent linear system will respond at that particular frequency with a certain magnitude and a certain phase angle relative to the that sine wave input. A system's frequency response is the Fourier transform of its impulse response. The frequency response of the transponder will be the quantitative measure of its output spectrum in response to the incident sine wave signal. It can prove to helpful while calculating the conversion efficiency or the ratio P_{OUT}/P_{IN} as it is a measure of the magnitude and phase of the output as a function of frequency compared to its input.

When only a single diode is used to rectify AC i.e. blocking the positive or negative portion of the waveform, the difference between the term diode and the term rectifier is simply one of usage. Rectification is basically a process in which a diode is used to convert AC to DC. In the case of the transponder fitted with a Schottky Barrier diode, the process of half wave rectification takes place where only the positive half of the AC is passed while the negative is blocked. The reason that it is 50% efficient is because one half of the input waveform reaches the output.

It must be noted here that there will be losses due to noise as well such as thermal noise, which further decrease the efficiency of the transponder. The phenomenon can become more clear after seeing figures 10.3-10.5. Thus, the graphical representation of the power spectral density is used as a tool to aid the process of calculating the conversion efficiency.

10.2 Half-wave rectification

The half-wave rectification refers to the one-way conductivity of a diode: when the input is a standard sine wave, the output obtains the positive half of the sine wave and the negative half is lost.
During the positive half cycle, the diode is in a forward biased state and conducts current to R (load resistor). A voltage is generated across the load, which is the same as the input AC signal for the positive half cycle.

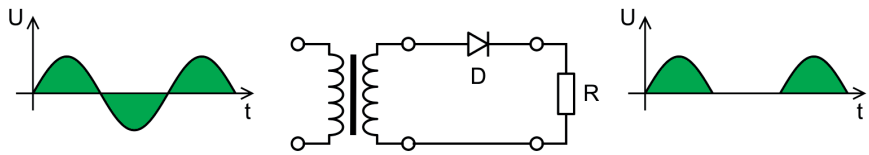

Figure 10.5: The model of half-wave rectification [15]

For a sinusoidal input voltage, the no-load output DC voltage of an ideal half-wave rectifier is:

$$V_{DC} = \frac{1}{\pi}\int_0^{\pi} V_{peak}\sin t dt = \frac{V_{peak}}{\pi} \tag{10.12}$$

$$V_{peak} = V_{rms}\sqrt{2} \tag{10.13}$$

$$V_{DC} = \frac{V_{peak}}{\pi} \tag{10.14}$$

Where V_{DC} refers to the output voltage, V_{peak} refers to the peak value of the input voltage and V_{rms} refers to the root mean square value of output voltage.

10.3 The RMS value of the voltage

RMS refers to the Root Mean Square value. The process is to sum all the values squared, find the mean value, and then square it to get the root mean square value. It is a mathematical method for defining the effective voltage or current of an AC wave.
The function of the rms value of the sine wave voltage can be written as:

$$U_{rms} = \sqrt{\frac{1}{\pi}\int_0^{2\pi} (U_m \sin\omega t)^2 d(\omega t)} = \frac{U}{\sqrt{2}} \tag{10.15}$$

For a sine wave voltage after diode half-wave rectification, the function of the rms value can be written as:

$$U_{rms} = \sqrt{\frac{1}{\pi}\int_0^{\pi} (U_m \sin\omega t)^2 d(\omega t)} = \frac{U}{2} \tag{10.16}$$

10.4 MATLAB Simulation results

In this part, a 100 Hz sine wave in time domain is generated first, followed by its frequency response. This is simulated as the waveform of an input voltage. As Fig. 10.6 shows below:

After rectification, since the diode only allows unidirectional current through the load characteristics, the positive current is blocked. The waveform of the output voltage and output current is the same as the waveform of the AC input

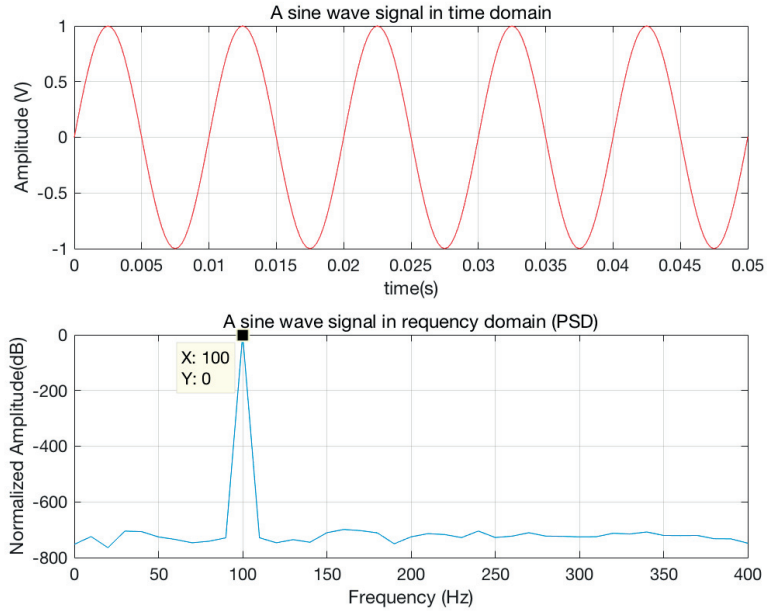

Figure 10.6: A 100Hz sine AC input waveform

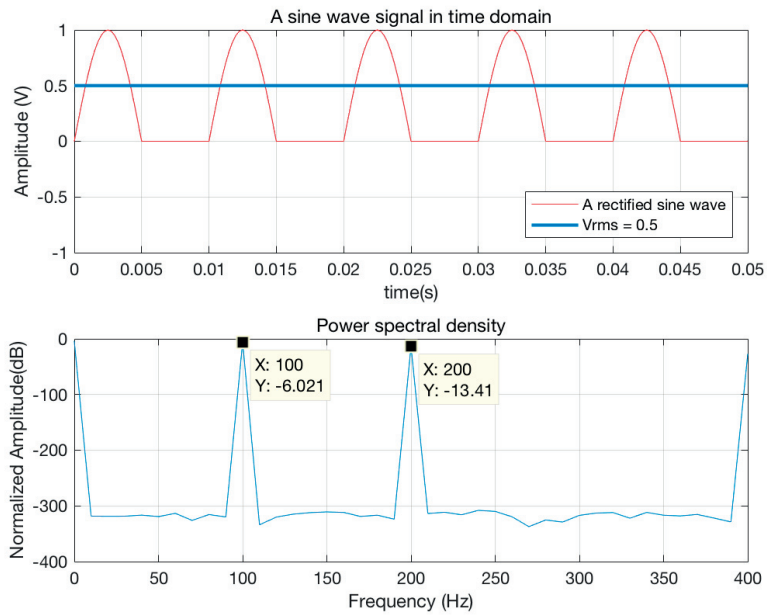

Figure 10.7: The waveform of half-wave rectification (ideal)

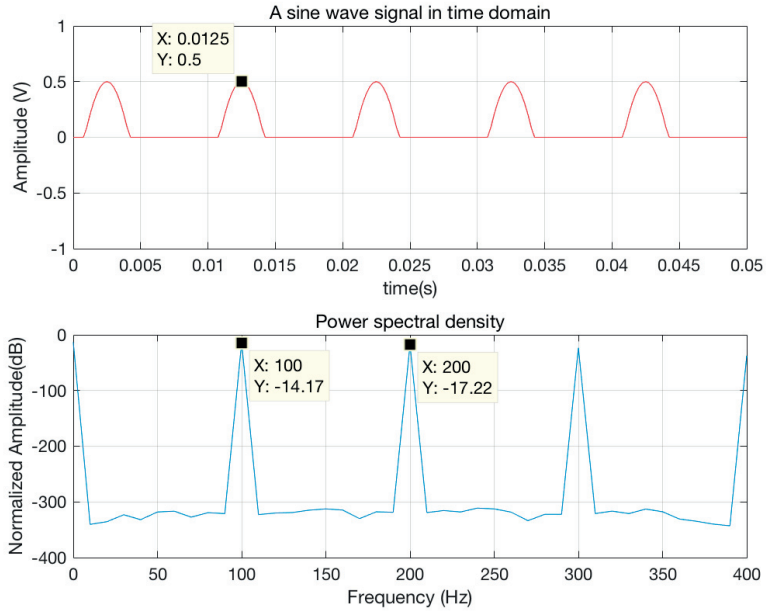

Figure 10.8: The waveform of half-wave rectification (realistic)

voltage, as shown in Figure 10.7, which is the ideal case. The value of V_{rms}=0.5 V.

However, in a real environment, since every diode requires a certain forward voltage V_F to switch on which is the voltage drop across the diode if the voltage at the anode is more positive than the voltage at the cathode, the results are a quite different from the previously mentioned ideal scenario. This is usually used to calculate the power dissipation of the diode and the voltage after the diode. A current thus flows through the diode if the applied voltage exceeds this value. In Fig. 10.6, the amplitude of the sine wave generated is 1 V, after this wave goes through the process of half wave rectification, the amplitude remains the same but the negative half is lost but when we account for the forward voltage the amplitude becomes 1 - V_f. There can always also be some loss during the conversion process in the transponder, for example, the thermal noise, transmitting loss due to circuit mismatching; or even the combination of them, so the values of V_{rms} and V_{DC} are less than the values in the ideal case, the model can be seen in Figure 10.8, where if V_F=0.5 V, the amplitude of the sine wave reduces to 0.5 V and the consequent power loss can then be seen as previously in the ideal case at 100 Hz we had -6 dB of power and -13 dB at at the second harmonic but after accounting for the forward voltage and taking into consideration the more realistic environment, the power at 100 Hz is -14 dB and -17 dB at the second harmonic.

10.5 Efficiency Calculation

Figure 10.9 shows the Second Harmonic Generation (SHG) conversion in a nonlinear material. To begin with, we have the power that is incident on the transponder from the transmitting antenna which is mentioned here as P_{in}. It is calculated before the rectification process i.e. before it passes through the diode. It is a normalized value, therefore:

$$P_{in} = 0 \quad \text{dB} \quad (normalized) \tag{10.17}$$

Secondly, P_{out}, the harmonic frequency at 200Hz, can observed from Figure 10.7 and 10.8, therefore:

$$P_{out} = -13.41 \quad \text{dB} \quad \text{(ideal)} \tag{10.18}$$

$$P_{out} = -17.22 \quad \text{dB} \quad \text{(realistic)} \tag{10.19}$$

Finally, we calculate the ratio between P_{out}/P_{in}:

$$\frac{p_{out}}{p_{in}}|_{linear} = p_{out}|_{dB} - p_{in}|_{dB} = -13.41 - 0 = -13.41 \quad \text{dB} \quad \text{(ideal)} \tag{10.20}$$

$$\frac{p_{out}}{p_{in}}|_{linear} = p_{out}|_{dB} - p_{in}|_{dB} = -17.22 - 0 = -17.22 \quad \text{dB} \quad \text{(realistic)} \tag{10.21}$$

Figure 10.9: The Second Harmonic Generation(SHG) conversion in a nonlinear material [16]

Normally, for most equipment in real life, they are designed to avoid a second harmonic signal generation because a second harmonic signal is very harmful. Harmonics will reduce the efficiency of the production, transmission of electrical energy, causing electrical equipment to overheat, generating vibration and noise, aging insulation, shortening service life, and even malfunctioning or burning.

In table 10.1, the system performance is summarized in terms of power during the second harmonic generation process. For the second harmonic in the ideal case, the efficiency after the conversion loss becomes -13.41 dB (21.35%), for the realistic environment case, the efficiency is -17.22 dB (13.77%) after the conversion loss.

G_{TX}	$G_{9.41GHz}$	L_c(ideal)
21.1 dBi	1.12 dBi	-13.41 dB
G_{RX}	$G_{18.82GHZ}$	L_c(realistic)
26.2 dBi	5.41 dBi	-17.22 dB

Table 10.1: The overall power consumption

10.6 Conclusion

The aim of this project was to design light weight antennas for a harmonic radar system that would help in understanding the navigation capabilities of the Bogong moths. The main challenges revolved around the size restrictions of the antennas. All three antennas designed in the end complied with the requirements of weight and size set in the beginning of the project by the research group from the Biology department. Two high gain and extremely narrow beam width patch antenna arrays were designed and fabricated, namely the Tx patch antenna array and the Rx patch antenna array, having gains 21.5 dB and 25 dB respectively with matching beam width of 11°.The final part of the thesis was to design a novel environmentally friendly transponder which whilst being light weight had a higher gain than the previous attempts made in this direction. The simulations were done with the body of the placed next to the transponder designed in order to get more accurate results which to the best of the authors' knowledge has not been done before. Finally, we have explained and presented the propagation model of the harmonic radar taking into account the more realistic environment that we live in and studied the conversion efficiency of the non-linearity that would be introduced in the transponder design which also forms the basis of it.

10.7 Future Work

Although results from our work have been promising, there are still a lot of improvements that can be made, one of which that we did not investigate due to the shortage of time was the two advanced feeding techniques for patch antennas, namely, aperture coupled feeding and proximity coupled feeding. It can be interesting to see whether they can prove to be as efficient or even more so than the inset feeding technique used in this project. The room for improvement and further work on the transponder side is even greater as the simulated designs were not fabricated at the time due to unavailability of resources. It can also be said that fitting the actual Bogong moths with the designed transponder and testing the antenna parameters and performance in real life can be something that would be of great value and understanding.

References

[1] Masconzoni and Wallin, "*The harmonic radar: a new method of tracing insects in the field*," Department of Radioecology, and Department of Plant and Forest Protection, Swedish University of Agricultural Sciences, Uppsala, Sweden, Ecological Entomology (1986) 11, 387-390

[2] Riley and Smith, "*Design considerations for an harmonic radar to investigate the flight of insects at low altitude*, " Plant and Invertebrate Ecology Division, IACR-Rothamsted, Harpenden, Hertfordshire AL5 2JQ, UK

[3] Colpitts and Boiteau, "*Harmonic Radar Transceiver Design: Miniature Tags for Insect Tracking*," IEEE Transactions On Antennas And Propagation, Vol. 52, No. 11, November 2004

[4] Milanesio, Saccani, Maggiora, Laurino and Porporato, "*Design of an harmonic radar for the tracking of the Asian yellow-legged hornet*",

[5] 1 Dipartimento di Elettronica e Telecomunicazioni (DET), Politecnico di Torino, Torino, Italy; Dipartimento di Scienze Agrarie, Forestali e Alimentari (DISAFA), Università degli Studi di Torino, Torino, Italy

[6] Riley, Valeur, Smith, Reynolds, Poppy and Lofstedt, "*Harmonic Radar as a Means of Tracking the Pheromone-Finding and Pheromone-Following Flight of Male Moths*"

[7] Psychoudakis, Moulder, Chen, Zhu and Volakis, "*A portable low-power harmonic radar system and conformal tag for insect tracking*," IEEE Antennas and Wireless Propagation Letters, vol. 7, pp. 444–447, 2008.

[8] Kiriazi, Nakakura, Hall, Hafner and Lubecke, "*Low Profile harmonic radar transponder for tracking small endangered species*," in Proceedings of the 29th Annual International Conference of the IEEE Engineering in Medicine and Biology Society (EMBS '07), pp. 2339–2441, IEEE, Lyon, France, August 2007.

[9] Nassar, Weller and Frolik, "*A compact 3-D harmonic repeater for passive wireless sensing*," IEEE Transactions on Microwave Theory and Techniques, vol. 60, no. 10, pp. 3309– 3316, 2012.

[10] Stutzman and Thiele, "*Antenna Theory and Design*" 3rd Edition

[11] Balanis, "*Antenna Theory, Analysis and Design*" 3rd Edition

[12] Abdennaceur and Badri, "*Design and Simulation of Microstrip Patch Array Antenna with High Directivity for 10 GHz Applications*," in International Symposium on Signal Image Video and Communications At: Marrakech, Maroc, IEEE, November 2010.

[13] Tahir and Brooker, "*Toward the Development of Millimeter Wave Harmonic Sensors for Tracking Small Insects*," in IEEE Sensors Journal Volume: 15, Issue: 10, October, 2015.

[14] Rasilainen, Ilvonen, Lehtovuori, Hannula and Viikari, "*On Design and Evaluation of Harmonic Transponders*", in IEEE Transactions on Antennas and Propagation Volume: 63, Issue: 1, January, 2015.

[15] Halfwave rectifier `https://upload.wikimedia.org/wikipedia/commons/5/58/Halfwave.rectifier.en.svg`

[16] Schematic of the SHG conversion of an excited wave in a non-linear medium `https://en.wikipedia.org/wiki/File:Schematic_of_the_SHG_conversion_of_an_excited_wave_in_a_non-linear_medium.png`

[17] Prof. Sean Victor Hum, Radio and Microwave Wireless Systems, Department of Electrical and Computer Engineering `http://www.waves.utoronto.ca/prof/svhum/ece422/notes/13-folded.pdf`

[18] Quarter wave impedance transformer `https://en.wikipedia.org/wiki/File:Quarter_wave_impedance_transformer.svg`

[19] Anders J Johansson, Department of EIT, Faculty of Engineering, LTH, Lund Univeristy `https://www.eit.lth.se/fileadmin/eit/courses/etin15/slides2017/Lecture02_Propagation_2017.pdf`

Printed by Tryckeriet i E-huset, Lund 2018

LUND
UNIVERSITY

Series of Master's theses
Department of Electrical and Information Technology
LU/LTH-EIT 2018-671
http://www.eit.lth.se